8-17-2023

# A Comparison of Battery Equivalent Circuit Model Parameter Extraction Approaches Based on Electrochemical Impedance Spectroscopy

Yuchao Wu
*University of Windsor*

# A COMPARISON OF BATTERY EQUIVALENT CIRCUIT MODEL PARAMETER EXTRACTION APPROACHES BASED ON ELECTROCHEMICAL IMPEDANCE SPECTROSCOPY

by

Yuchao Wu

A Thesis
Submitted to the Faculty of Graduate Studies
through the Department of Electrical and Computer Engineering
in Partial Fulfilment of the Requirements for
the Degree of Master of Applied Science at the
University of Windsor

Windsor, Ontario, Canada

A Comparison of Battery Equivalent Circuit Model Parameter Extraction Approaches Based on Electrochemical Impedance Spectroscopy

by

Yuchao Wu

APPROVED BY:

---

G. Rankin
Department of Mechanical, Automotive and Materials Engineering

---

X. Chen
Department of Electrical and Computer Engineering

---

B. Balasingam, Advisor
Department of Electrical and Computer Engineering

August 3, 2023

# Declaration of Co-Authorship / Previous Publication

## Co-Authorship

I hereby declare that this thesis incorporates material that is result of joint research, as follows: Chapter 2 of this thesis includes the outcome of publication which has the following other co-authors: S. Sundaresan and B. Balasingam. In all cases only my primary contributions towards this publication are included in this thesis, S. Sundaresan provided assistance in investigation and experimentation, B. Balasingam contributed to experimental design, conceptualization, review and editing of the manuscript. Chapter 2 of this thesis also incorporates unpublished material co-authored with B. Balasingam. In all cases, the key ideas, primary contributions, experimental designs, data analysis, interpretation, and writing were performed by myself, B. Balasingam contributed to review and editing of the manuscript.

I am aware of the University of Windsor Senate Policy on Authorship and I certify that I have properly acknowledged the contribution of other researchers to my thesis, and have obtained written permission from each of the co-author(s) to include the above material(s) in my thesis.

# Previous Publication

| Thesis chapter | Publication title/full citation | Publication status | Journal |
|---|---|---|---|
| 2 | Y. Wu, S. Sundaresan, and B. Balasingam, "Battery parameter analysis through electrochemical impedance spectroscopy at different state of charge levels," J. Low Power Electron. Appl., vol. 13, no. 2, p. 29, 2023. | Published | J. Low Power Electron. Appl. |
| 2 | Y. Wu and B. Balasingam, "A Comparison of Battery Equivalent Circuit Model Parameter Extraction Approaches Based on Electrochemical Impedance Spectroscopy," IEEE Transactions on Transportation Electrification, 2023. | Under review | IEEE Transactions on Transportation Electrification |

I certify that I have obtained a written permission from the copyright owner(s) to include the above published material(s) in my thesis. I certify that the above material describes work completed during my registration as a graduate student at the University of Windsor.

# General

I declare that, to the best of my knowledge, my thesis does not infringe upon anyone's copyright nor violate any proprietary rights and that any ideas, techniques, quotations, or any other material from the work of other people included in my thesis, published or otherwise, are fully acknowledged in accordance with the standard referencing practices. Furthermore, to the extent that I have included copyrighted material that surpasses the bounds of fair dealing within the meaning of the Canada Copyright Act, I certify that I have obtained a written permission from the copyright owner(s) to include such material(s) in my thesis. I declare that this is a true copy of my thesis, including any final revisions, as approved by my thesis committee and

the Graduate Studies office, and that this thesis has not been submitted for a higher degree to any other University or Institution.

# Abstract

This thesis compares three methods for estimating battery parameters of the electrical equivalent circuit model (ECM) based on electrochemical impedance spectroscopy (EIS). These methods are referred to as least squares (LS), exhaustive search (ES), and nonlinear least squares (NLS). The ES approach utilizes the LS method to roughly determine the lower and upper bounds of the ECM parameters, while the NLS approach incorporates a Monte Carlo run, allowing for different initial guesses to enhance the accuracy of EIS fitting. The proposed approaches are validated using both simulated and real-world EIS data. When the signal-to-noise ratio (SNR) is high, both the ES and NLS approaches exhibit better fitting accuracy compared to the LS approach. Furthermore, in the validation using simulated EIS data as well as actual EIS data obtained from LG 18650 and Molicel 21700 batteries, the NLS approach consistently outperforms the LS and ES approaches in terms of fitting accuracy. Additionally, the computational time required for the NLS approach is significantly shorter than that of the ES approach, and the NLS approach demonstrates only a minimal difference in computational time compared to the LS approach while providing significantly better fitting performance.

# Contents

# List of Tables

# List of Figures

# Chapter 1

# Introduction

## 1.1 The Application of Battery Management System (BMS)

The BMS is crucial in modern battery-based energy storage systems. Its primary objective is to guarantee the secure and effective functioning of the battery pack by overseeing and regulating multiple parameters; it is also critical in optimizing battery performance, extending longevity, and minimizing potential safety hazards [1].

Electric vehicles (EVs) represent a significant application area for BMS. Within EVs, BMS actively monitors individual cells' voltages, temperatures, and state of charge [2]. This monitoring process aims to optimize the battery's overall performance and prevent potentially hazardous situations such as overcharging or over-discharging. Additionally, BMSs play a crucial role in voltage balancing by redistributing the charge among cells, ensuring uniformity and enhancing the overall efficiency of the battery. Moreover, BMS can provide the range an EV can travel on a single charge and diagnose the battery's overall health [3]. Fig. 1.1 illustrates the main features of a BMS [4].

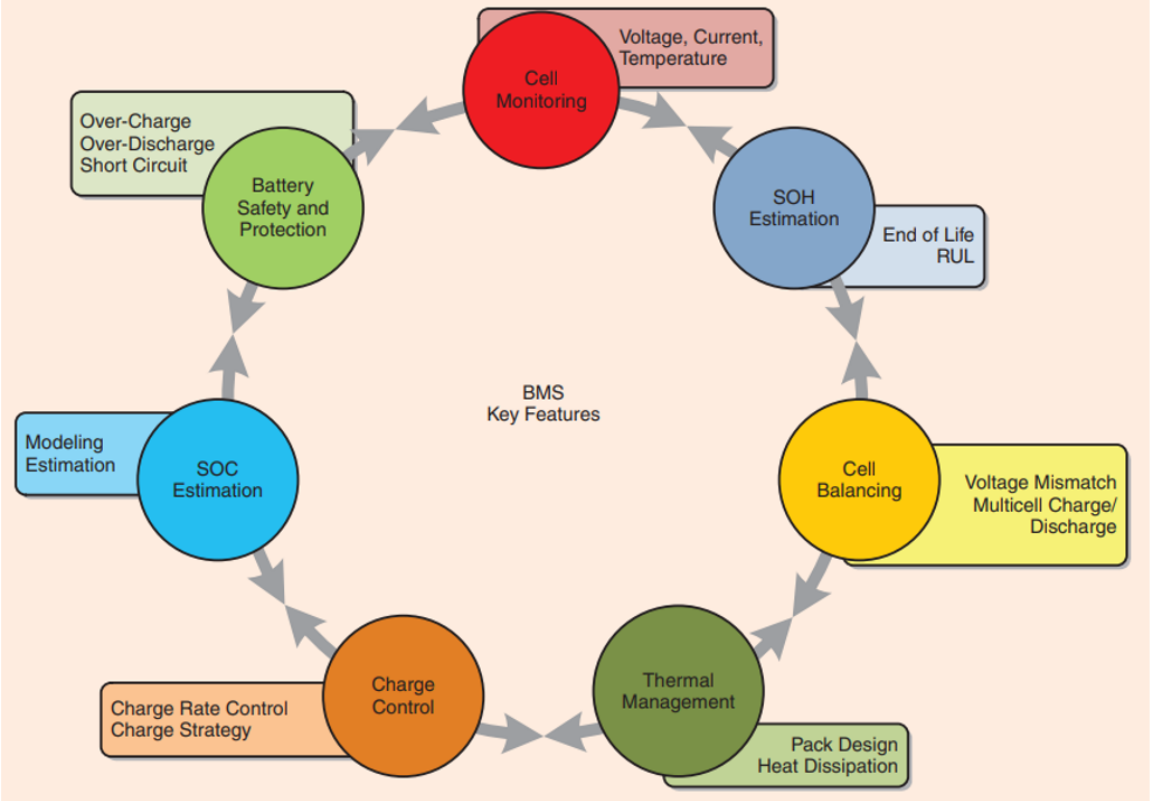


Figure 1.1: **Key features of BMS [4].**

## 1.2 The Importance of Electrochemical Impedance Spectroscopy (EIS) in BMS

Electrochemical impedance spectroscopy (EIS) is widely used to provide useful information relevant to the battery's chemical-physical properties, which can impact battery aging or failure events [5].

Characterizing the impedance is crucial for determining the operational limits of a battery, evaluating its performance, and monitoring its state of health (SOH) [6, 7], state of charge (SOC) [8, 9], and internal temperature [10]. Moreover, EIS can be used for grading battery packs for its second-life applications [11]. Furthermore, EIS is a non-invasive method that can be applied at any stage of the battery's lifespan without causing damage [12].

## 1.3 Identification of Battery Equivalent Circuit Model (ECM) Parameters via EIS

EIS provides valuable information about the internal processes occurring within a battery by measuring its impedance response to an applied sinusoidal excitation signal. EIS can be employed to determine the parameters (resistance, capacitance, and inductance) of the ECM [13], representing the battery's electrochemical behaviour. However, identifying ECM parameters via battery EIS poses several challenges to overcome for accurate characterization.

The behavior of batteries shows nonlinear effects such as diffusion limitations, concentration polarization, and nonlinear electrode kinetics that can significantly impact the impedance spectroscopy [14]. Neglecting these nonlinearities may lead to inaccurate parameter estimation of ECM; as a result, advanced ECMs that consider nonlinear phenomena, such as Warburg elements and double-layer capacitances, need to be employed [12].

In addition, EIS measurements are susceptible to various defects and noise sources that can compromise the accuracy of parameter identification. Factors such as stray inductance, contact resistances, cable impedance, and thermal gradients can introduce unwanted distortions in the impedance spectra. Proper experimental setup, including careful sample preparation, high-quality instrumentation, and robust data analysis techniques, is necessary to minimize these errors [15].

Furthermore, the identification of ECM parameters from EIS data is an inverse problem that often suffers from parameter correlation; different combinations of ECM parameters can yield similar impedance spectroscopy, making it challenging to uniquely determine the true values; as a result, advanced parameter estimation techniques are required to improve parameter identifiability.

## 1.4 Organization of the Thesis

The thesis is presented in the manuscript format with three Chapters.

The remainder of this thesis is organized as follows: Chapter 2 details the performance comparisons of three approaches, i.e., LS, ES, and NLS, to extract battery ECM parameters based on the EIS data simulated via MATLAB and on the EIS data collected from LG and Molicel batteries. Chapter 3 concludes the thesis.

## 1.5 Bibliography


[1] Y. Xing, E. W. M. Ma, K. L. Tsui, and M. Pecht, "Battery management systems in electric and hybrid vehicles," *Energies*, vol. 4, no. 11, pp. 1840–1857, 2011.

[2] H. Ren, Y. Zhao, S. Chen, and T. Wang, "Design and implementation of a battery management system with active charge balance based on the SOC and SOH online estimation," *Energy (Oxf.)*, vol. 166, pp. 908–917, 2019.

[3] L. Lu, X. Han, J. Li, J. Hua, and M. Ouyang, "A review on the key issues for lithium-ion battery management in electric vehicles," *J. Power Sources*, vol. 226, pp. 272–288, 2013.

[4] H. Rahimi-Eichi, U. Ojha, F. Baronti, and M.-Y. Chow, "Battery management system: An overview of its application in the smart grid and electric vehicles," *IEEE Ind. Electron. Mag.*, vol. 7, no. 2, pp. 4–16, 2013.

[5] K. W. Beard, *Linden's handbook of batteries, fifth edition*, 5th ed. Columbus, OH: McGraw-Hill Education, 2019.

[6] S. Rodrigues, N. Munichandraiah, and A. K. Shukla, "AC impedance and state-of-charge analysis of a sealed lithium-ion rechargeable battery," *J. Solid State Electrochem.*, vol. 3, no. 7–8, pp. 397–405, 1999.

[7] S. F. Schuster, M. J. Brand, C. Campestrini, M. Gleissenberger, and A. Jossen, "Correlation between capacity and impedance of lithium-ion cells during calendar and cycle life," *J. Power Sources.*, vol. 305, pp. 191–199, 2016.

[8] R. Xiong, J. Tian, H. Mu, and C. Wang, "A systematic model-based degradation behavior recognition and health monitoring method for lithium-ion batteries," *Appl. Energy*, vol. 207, pp. 372–383, 2017.

[9] A. Cuadras and O. Kanoun, "SoC Li-ion battery monitoring with impedance spectroscopy," in *2009 6th International Multi-Conference on Systems, Signals and Devices*, 2009.

[10] L. H. J. Raijmakers, D. L. Danilov, J. P. M. van Lammeren, M. J. G. Lammers, and P. H. L. Notten, "Sensorless battery temperature measurements based on electrochemical impedance spectroscopy," *J. Power Sources*, vol. 247, pp. 539–544, 2014.

[11] Q. Liao et al., "Performance assessment and classification of retired lithium ion battery from electric vehicles for energy storage," *Int. J. Hydrogen Energy*, vol. 247, pp. 539–544, 2014.

[12] N. Meddings et al., "Application of electrochemical impedance spectroscopy to commercial Li-ion cells: A review," *J. Power Sources*, vol. 480, no. 228742, p. 228742, 2020.

[13] E. Barsoukov, *Impedance Spectroscopy: Theory, Experiment, and Applications*, Wiley, 2018.

[14] F. Fasmin and R. Srinivasan, "Review—nonlinear electrochemical impedance spectroscopy," *J. Electrochem. Soc.*, vol. 164, no. 7, pp. H443–H455, 2017.

[15] "Theory behind cable-capacitance correction," *Gamry.com.*, [Online]. Available: https://www.gamry.com/Framework [Accessed: 11-Jul-2023].

# Chapter 2

# Comparison of Approaches to Battery ECM Parameters Estimation Based on EIS

## 2.1 Introduction

A Battery Management System (BMS) is a crucial component in electric vehicles (EVs), renewable energy systems, and other applications that use rechargeable batteries to ensure safe and efficient operation. The primary function of a BMS is to monitor the battery's state of charge (SOC) and state of health (SOH) [1]. Electrochemical impedance spectroscopy (EIS) was proposed by Heaviside 1894 [2]; it has become an essential tool in the study and development of batteries; this allows researchers to better understand the fundamental electrochemical mechanisms such that correct strategies can be implemented in BMS for improving battery performance and lifespan.

EIS has been used to study the ion transport properties and electrode/electrolyte interfacial behavior of Li-ion batteries, providing insights into their performance and potential avenues for improvement [3]. In a typical EIS experiment, a small amplitude sinusoidal current/voltage signal is applied to the battery, and the resulting voltage/current response is measured over a range of frequencies [4]. The resulting impedance data can be analyzed using equivalent electrical circuit models to extract information on the underlying electrochemical behavior [5]. EIS can provide detailed information on the electrochemical processes occurring within the battery, including the charge transfer kinetics, ion transport properties, and electrode/electrolyte interfacial behavior [6]. Pastor-Fernández *et al.* [7] conducted the battery aging identification and quantification research by analyzing the EIS of four parallel Li-ion cells.

The EIS can be characterized using an equivalent circuit model (ECM), which represents the battery as a combination of resistive, inductive, and capacitive components; then, the ECM parameters can be identified by fitting the ECM to the measured EIS data [8]. There are different ECM models relevant to different types of batteries; this requires prior knowledge of the battery chemistry [9]; furthermore, by iteratively adjusting the ECM parameters, the best fit can be obtained.

There are various approaches to fit the ECM model to the measured EIS data. For instance, nonlinear least squares (NLS) approach can be used to estimate the parameters of a nonlinear model; this aims to optimize the nonlinear function such that the difference between experimental data and the estimations based on the ECM model can be minimized [10]. Xu *et al.* [11] applied a NLS approach to fit the EIS data of a supercapacitor using the ECM model; this approach can identify the ECM parameters by minimizing the error between measurements and predictions.

Artificial Neural Network (ANN) can also identify the ECM parameters. Xu *et al.* [12] used ANN-based EIS fitting approach to predict the impedance of battery at different frequencies.

Besides, Genetic Algorithm (GA) is a population-based optimization approach that can also be used in fitting the ECM to EIS data; however, the computational complexity of this approach will increase significantly with the number of ECM parameters, which means that a large number of iterations are needed; furthermore, the selection of population size, mutation rate, and crossover rate requires continuous tuning to reach the optimal estimation [13].

The complex nonlinear least squares (CNLS) approach is widely used to fit the ECM model to EIS data. Pastor-Fernández *et al.* [7] applied the CNLS algorithm to fit ECM to the EIS data measured from four Lion-ion batteries. Feng *et al.* [14] applied CNLS approach to estimate ECM parameters using the EIS data collected from a battery cell at different SOC levels and temperatures. The drawback of this approach is that the fitting accuracy can easily be affected by the initial guess of the ECM parameters; for instance, the optimization algorithm may converge to a local minimum instead of converging to a global minimum if the initial guess is selected inappropriately; this will lead to inaccurate ECM parameter estimation. Also, CNLS approach requires the specification of ECM models, such as the number of components and the arrangement of RC circuits, which leads to extra work being done before the fitting process; furthermore, CNLS is a computationally expensive approach,

especially when the size of EIS measurements are large [15].

Ghadi [16] applied the least squares (LS) approach to fit the EIS data to identify ECM parameters by assuming the solid electrolyte interface (SEI) arc and charge transfer (CT) arc as semicircle, and the solid electrolyte interface resistance $R_{SEI}$ and charge transfer resistance $R_{CT}$ is the diameter of the SEI arc and the CT arc, respectively; the merit of this approach is that the estimation of the parameters can be expressed in closed form; however, the main drawback is that the accuracy of this approach is not sufficient. One of the improvements is to apply the exhaustive search (ES) approach to identify more accurate estimations of ECM parameters with the assistance of LS approach.

In this chapter, we proposed a novel NLS approach which only needs to define the objective function at the beginning, then randomly select the initial guess in each Monte-Carlo run to achieve the best fitting accuracy. Besides, the computational time is around 2 seconds, which is very promising in fitting real battery's EIS data. While the ES approach can reach a better fitting accuracy compared with the LS approach, the computational time is still very slow. As a result, the NLS approach based on Monte-Carlo run can be applied for the extraction of ECM parameters.

The contributions of this chapter can be summarized as follows:

1. This chapter compares the performance of the LS, ES, and Monte-Carlo-based NLS approaches to identifying battery ECM parameters.

2. Compared to the LS approach presented in [16], the ES and the NLS approach can significantly boost the fitting accuracy of EIS measurements.

3. This chapter presents a novel approach to implementing NLS through Monte Carlo runs. At each Monte Carlo run, the initial parameters required for the NLS approach are selected randomly. This approach results in better accuracy and much faster computation time than the ES approach.

4. All the methods are validated in simulated EIS data with different SNRs and

are also validated in actual EIS data collected from two different types of Li-ion batteries, the fitting performance of the NLS approach outweighs other approaches in all cases.

The remainder of this chapter is organized as follows: Section 2.2 describes the analysis of battery ECM parameters via EIS in the frequency domain. Section 2.3 describes the algorithms to estimate ECM parameters using the least squares approach. Section 2.4 describes algorithms of exhaustive search, the Monte-Carlo-based nonlinear least squares approach is explained in section 2.5. Implementation procedure is explained in section 2.6. Results are discussed in section 2.7. Section 2.8 concludes this chapter.

## 2.2 Analysis of ECM Parameters in Frequency Domain

EIS is a widely used technique to investigate the impedance response of the battery. As shown in Fig. 2.2 [17], to measure the EIS, a small perturbation voltage or current with a wide range of frequencies (0.01 Hz to 10 kHz) is injected to the battery; then, by using Fast Fourier Transform (FFT), the measured voltage and current in the time domain can be converted to the frequency domain; thus, the impedance in the frequency domain can be analyzed [18, 19]. The battery impedance can then be represented by the real part of the impedance and the imaginary part of the impedance on the complex plane to form the Nyquist plot [20, 21]. This plot represents the impedance spectrum of the battery at a range of frequencies; the ECM parameters can be estimated by fitting the EIS data with suitable fitting algorithms.

The frequency domain approach uses the Adaptive Randles (AR) ECM shown in Fig. 2.3. The AR-ECM consists of the following components [19]:

- Voltage Source, EMF

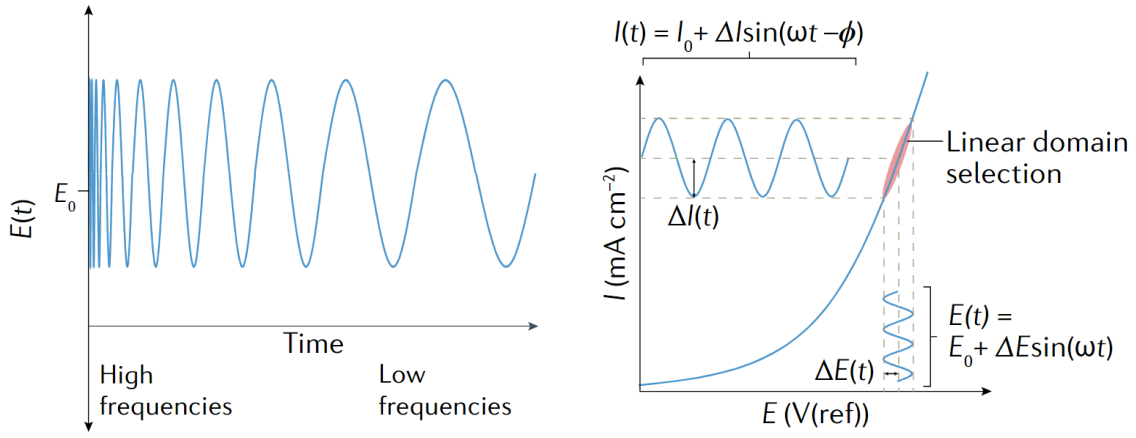


(a) (b)

Figure 2.2: **EIS Measurement [17].** (a) Perturbation signal. (b) Electrochemical response.

- Stray Inductance, $L$
- Ohmic Resistance, $R_\Omega$
- Solid Electrolytic Interface (SEI) Resistance, $R_{SEI}$
- SEI Capacitance, $C_{SEI}$
- Charge Transfer (CT) resistance, $R_{CT}$
- Double Layer (DL) Capacitance, $C_{DL}$
- Warburg Impedance, $Z_{\mathrm{W}}$

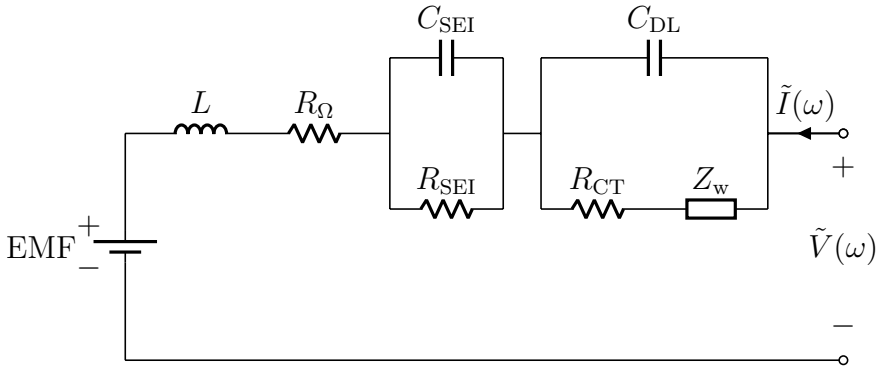


Figure 2.3: **Adaptive Randles equivalent circuit model (AR-ECM) of a battery.**

Fig. 2.4 shows the Nyquist plot relevant to the AR-ECM. According to this figure, the AC impedance $Z(w)$ corresponding to the AR-ECM can be written as [16]

$$\begin{aligned} Z(\omega) &\triangleq Z(j\omega) \\ &= j\omega L + R_\Omega + \frac{1}{\frac{1}{R_{\mathrm{SEI}}} + j\omega C_{\mathrm{SEI}}} + \frac{1}{\frac{1}{R_{\mathrm{CT}}+Z_{\mathrm{w}}(j\omega)} + j\omega C_{\mathrm{DL}}} \\ &= \underbrace{j\omega L + R_\Omega}_{Z_{\mathrm{RL}}} + \underbrace{\frac{R_{\mathrm{SEI}}}{1 + j\omega R_{\mathrm{SEI}} C_{\mathrm{SEI}}}}_{Z_{\mathrm{SEI}}} + \underbrace{\frac{R_{\mathrm{CT}} + Z_{\mathrm{w}}(j\omega)}{1 + j\omega \left(R_{\mathrm{CT}} + Z_{\mathrm{w}}(j\omega)\right) C_{\mathrm{DL}}}}_{Z_{\mathrm{CT\&DF}}} \end{aligned} \tag{2.1}$$

Where $Z_{\mathrm{RL}}$ denotes the impedance in the RL arc, $Z_{\mathrm{SEI}}$ denotes the impedance in the SEI arc, and $Z_{\mathrm{CT\&DF}}$ denotes the impedance in the CT arc and DF arc.

## 2.3 Least Squares Approach

To solve the problem of ECM parameter estimation, Ghadi [16] applied the LS algorithm to fit the EIS measurements; furthermore, this approach can express the estimation of ECM parameters in closed form. In this section, an improved LS approach to AR-ECM parameter estimation is presented.

Fig. 2.4 shows the impedance spectrum/Nyquist plot corresponding to the AR-ECM shown in Fig. 2.3. Each data point in the Nyquist plot is obtained through the procedure as shown in Fig. 2.5, where $z_v(t)$ and $z_c(t)$ are the measured voltage and current in the time domain while injecting sinusoidal current to the battery at different frequencies; $Z_v(\omega)$ and $Z_c(\omega)$ are the Fourier transform of the corresponding voltage and current measurements.

It can be observed that the Nyquist plot needs to be divided into four parts to see how it is directly related to the AR-ECM. The feature points of the Nyquist plot are indicated by index $k_{DF1}$ and $k_{DF2}$ in the DF arc; are indicated by $k_{CT1}$ and $k_{CT2}$ in the CT arc; are indicated by $k_{SEI1}$ and $k_{SEI2}$ in the SEI arc; and are indicated by $k_{RL1}$ and $k_{RL2}$ in the RL arc. Different parts of the Nyquist plot represent the battery's

impedance at different frequencies [22]. In this chapter, to keep the consistency of nomenclature, we define:

- $k_{DF1}$ is the index of the first data point in the DF arc, in this chapter, we define $k_{DF1} = 1$.
- $k_{DF2}$ is selected such that the data points from $k_{DF1}$ to $k_{DF2}$ follows the linear line.
- $k_{CT1}$ is selected at the beginning of the CT arc such that the data points start to follow the arc.
- $k_{CT2}$ is selected at the end of the CT arc such that data points between $k_{CT1}$ *and* $k_{CT2}$ follow the CT arc.
- Similarly, $k_{SEI1}$ is selected at the beginning of the SEI arc.
- $k_{SEI2}$ is selected at the end of the SEI arc such that data points between $k_{SEI1}$ *and* $k_{SEI2}$ follow the SEI arc.
- $k_{RL1}$ is selected at the beginning of the RL arc.
- $k_{RL2}$ is selected at the end of the RL arc.

### 2.3.1 Estimation of Ohmic Resistance and Stray Inductance

As shown in Fig. 2.4, based on the impedance measurements in the RL arc, the ohmic resistance $R_\Omega$ can be estimated as

$$\hat{R}_\Omega = \frac{1}{k_{RL2} - k_{RL1} + 1} \sum_{k=k_{RL1}}^{k_{RL2}} z_r(k) \tag{2.2}$$

and stray inductance $L$ can be estimated using the improved method:

$$\hat{L} = \frac{z_i(k_{RL2})}{\omega_{k_{RL2}}} \tag{2.3}$$

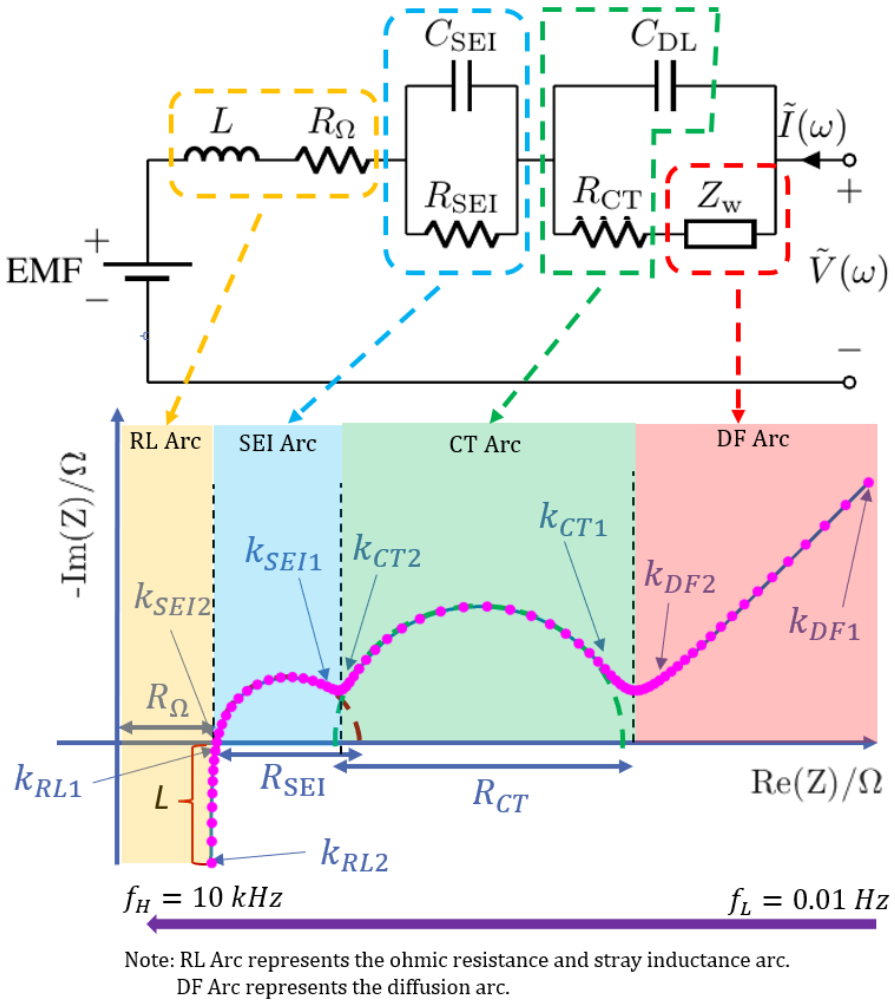


Figure 2.4: **The theoretical Nyquist plot corresponding to the AR-ECM.**

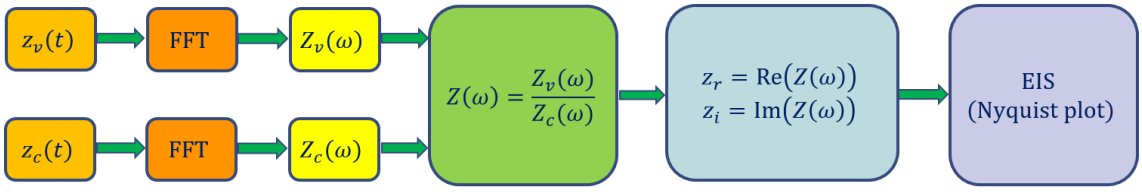


Figure 2.5: **The procedure to obtain EIS.**

where as shown in Fig. 2.5,

$$z_r(k) = Re(Z(\omega_k)), \quad z_i(k) = Im(Z(\omega_k)), \tag{2.4}$$

and $\omega_{k_{RL1}} \leq \omega_k \leq \omega_{k_{RL2}}$.

### 2.3.2 Estimation of Diffusion Arc's Gradient $m$

Considering the imaginary part of the measured impedance $z_i(k)$ and the real part of the measured impedance $z_r(k)$ in the Diffusion arc, it can be represented with a linear model:

$$z_i(k) = mz_r(k) + a \tag{2.5}$$

Assuming the measurements are from $k_{DF1}$ to $k_{DF2}$ as shown in Fig. 2.4, the following can be written as

$$\begin{aligned} z_i(k_{DF1}) &= mz_r(k_{DF1}) + a \\ z_i(k_{DF1+1}) &= mz_r(k_{DF1+1}) + a \\ &\vdots \\ z_i(k_{DF2}) &= mz_r(k_{DF2}) + a \end{aligned} \tag{2.6}$$

Equation (2.6) can be written in the matrix form

$$\underbrace{\begin{bmatrix} z_i(k_{DF1}) \\ z_i(k_{DF1}+1) \\ \vdots \\ z_i(k_{DF2}) \end{bmatrix}}_{\mathbf{y}} = \underbrace{\begin{bmatrix} z_r(k_{DF1}) & 1 \\ z_r(k_{DF1}+1) & 1 \\ \vdots & \\ z_r(k_{DF2}) & 1 \end{bmatrix}}_{\mathbf{A}} \underbrace{\begin{bmatrix} m \\ a \end{bmatrix}}_{\mathbf{k}} \tag{2.7}$$

$m$ and $a$ can be estimated using the LS approach:

$$\hat{\mathbf{k}} = (\mathbf{A}^T\mathbf{A})^{-1}(\mathbf{A}^T\mathbf{y}) \tag{2.8}$$

$$\hat{m} = \hat{\mathbf{k}}(1), \quad \hat{a} = \hat{\mathbf{k}}(2) \tag{2.9}$$

Algorithm 1 estimates quantities (list) based on the following impedance values:

$$\mathbf{z}_r = [z_r(1), z_r(2), \ldots, z_r(n)] \tag{2.10}$$

$$\mathbf{z}_i = [z_i(1), z_i(2), \ldots, z_i(n)] \tag{2.11}$$

In this thesis, the uppermost bound of the DF arc is denoted as $k^H_{DF}$, the lowest bound of the CT arc is denoted as $k^L_{CT}$, and the lowest bound of the SEI arc is denoted as $k^L_{SEI}$, these boundaries can be identified by applying moving average filter (MAF) to process the measured impedance data via Algorithm 1, the filtered EIS data is shown in Fig. 2.6a. The algorithms presented in this chapter are written by utilizing MATLAB syntax. Algorithm 1 uses the following MATLAB commands: 'smooth', 'min' 'break', and 'continue'.

**Algorithm 1** Boundary identification.

**Input:** $\mathbf{z}_r$, $\mathbf{z}_i$.
**Output:** $k^L_{SEI}$, $k^L_{CT}$, $k^H_{DF}$

$\mathbf{s}_{zr} \leftarrow \text{smooth}(\mathbf{z}_\text{r}, 10)$
$\mathbf{s}_{zi} \leftarrow \text{smooth}(\mathbf{z}_\text{i}, 10)$
$iter = 0$
**while** true **do**
    $iter = iter + 1$
    **if** $(\mathbf{s}_{zi}(iter + 1) \geq \min(\mathbf{s}_{zi}(1 : iter)) \mid (iter \geq k_{SEI2})$ **then**
        $k^L_{SEI} \leftarrow iter + 10$
        $k^L_{CT} \leftarrow iter + 10$
        $k^H_{DF} \leftarrow iter$
        break
    **else**
        continue
    **end if**
**end while**

The gradient $m$ of the Diffusion arc can be estimated by fitting the Diffusion arc with the linear model mentioned in (2.5) and searching out the best fit using Algorithm 2. The fitting process is also demonstrated in Fig. 2.6b and 2.6c. Algorithm 2 uses the following MATLAB commands: 'mean', 'find', and 'max'.

**Algorithm 2** Diffusion arc fitting.

**Input:** $\mathbf{z}_r$, $\mathbf{z}_i$, $k_{DF}^H$
**Output:** $\hat{m}$, $k_{DF2}$

**for** $i = 1 : k_{DF}^H - 1$ **do**
  $z_r(k)$, $k = 1, 2, ..., i+1 \leftarrow \mathbf{z}_r(1 : i+1)$
  $z_i(k)$, $k = 1, 2, ..., i+1 \leftarrow \mathbf{z}_i(1 : i+1)$
  $\mathbf{m}(i) \leftarrow$ Estimate gradient in $i^{th}$ iteration via Eq. (2.5) - (2.9)
  $\hat{\mathbf{y}} \leftarrow$ Estimate imaginary part of the impedance based on the fitted linear model.
  $S_r = \sum_{k=1}^{i+1} (z_i(k) - \hat{\mathbf{y}}(k))^2$ ▷ the sum of error squares
  $S_t = \sum_{k=1}^{i+1} (z_i(k) - \text{mean}(\hat{\mathbf{y}}))^2$ ▷ the total sum of squares around the mean
  $\mathbf{r}(i) = \sqrt{\frac{S_t - S_r}{S_t}}$ ▷ correlation coefficient
**end for**
$k_{DF2} \leftarrow \text{find}(\mathbf{r} == \max(5 : \text{end}))$ ▷ written in MATLAB syntax
$\hat{m} \leftarrow \mathbf{m}(k_{DF2})$

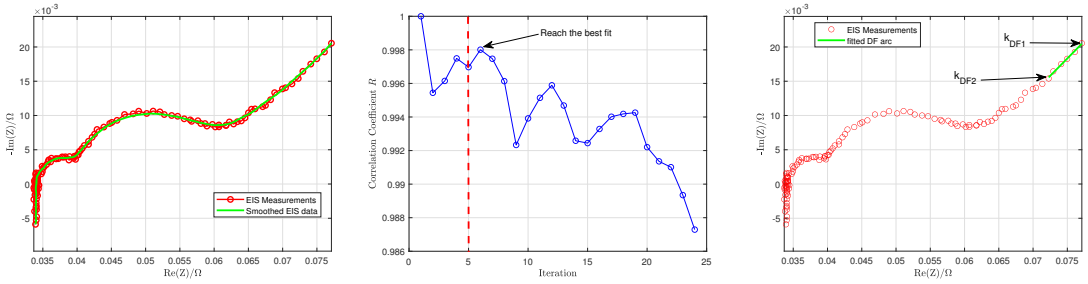


(a) (b) (c)

Figure 2.6: **DF arc fitting process.** (a) Smooth the EIS using MAF. (b) Find the highest correlation coefficient r when fitting the DF arc. (c) Fitted DF arc.

### 2.3.3 First Estimation of Warburg Coefficient $\sigma$

From the observation of EIS measurements in [22], it was found that the gradient of the Diffusion arc varies with the SOC level; in addition, gradients may be different even at the same SOC level of batteries from two different manufacturers; therefore, an improved method to represent Warburg impedance is defined mathematically as

$$Z_w(j\omega) = (1 - jm)\frac{\sigma}{\sqrt{\omega}} \tag{2.12}$$

where $\sigma$ is the Warburg coefficient, $m$ is the gradient of fitted DF arc, and $j$ is $\sqrt{-1}$.

It must be emphasized here that in [16] the gradient was assumed to be $m = 1$. In this chapter, it is proposed to estimate the gradient m to achieve better EIS fitting.

It can be shown based on (2.1) that the Warburg impedance is significant only at lower frequencies. In Fig. 2.4, impedance measurements from $k_{DF1}$ to $k_{DF2}$ are selected to estimate the Warburg coefficient (we define $k_{DF1} = 1$, and $k_{DF2}$ is obtained via Algorithm 2). Considering the real part of the impedance $z_r$ in the diffusion arc:

$$\begin{aligned} z_r(k_{DF1}) - z_r\left(k_{DF2}\right) &= \sigma\left(\frac{1}{\sqrt{\omega_{k_{DF1}}}} - \frac{1}{\sqrt{\omega_{k_{DF2}}}}\right) \\ z_r(2) - z_r\left(k_{DF2} - 1\right) &= \sigma\left(\frac{1}{\sqrt{\omega_2}} - \frac{1}{\sqrt{\omega_{(k_{DF2}-1)}}}\right) \\ &\vdots \\ z_r(n) - z_r\left(k_{DF2} - n + 1\right) &= \sigma\left(\frac{1}{\sqrt{\omega_n}} - \frac{1}{\sqrt{\omega_{(k_{DF2}-n+1)}}}\right) \end{aligned} \tag{2.13}$$

where $n = \lfloor \frac{k_{DF2}-k_{DF1}+1}{2} \rfloor$.

The observation model corresponding to (2.13) is

$$\tilde{\mathbf{z}} = \mathbf{b}\sigma \tag{2.14}$$

where

$$\tilde{\mathbf{z}} = \begin{bmatrix} z_r(1) - z_r\left(k_{DF2}\right) \\ z_r(2) - z_r\left(k_{DF2} - 1\right) \\ \vdots \\ z_r(n) - z_r\left(k_{DF2} - n + 1\right) \end{bmatrix},$$

$$\mathbf{b} = \begin{bmatrix} \left(\frac{1}{\sqrt{\omega_1}} - \frac{1}{\sqrt{\omega_{k_{DF2}}}}\right) \\ \left(\frac{1}{\sqrt{\omega_2}} - \frac{1}{\sqrt{\omega_{(k_{DF2}-1)}}}\right) \\ \vdots \\ \left(\frac{1}{\sqrt{\omega_n}} - \frac{1}{\sqrt{\omega_{(k_{DF2}-n+1)}}}\right) \end{bmatrix}$$

and the LS estimate of $\sigma$ is

$$\hat{\sigma}_{LS} = (\mathbf{b}^T\mathbf{b})^{-1}(\mathbf{b}^T\tilde{\mathbf{z}}) \tag{2.15}$$

### 2.3.4 Estimation of $R_{\text{SEI}}$ and $C_{\text{SEI}}$

As shown in Fig. 2.4, to fit the SEI arc precisely, we select feature points that lie between $k_{SEI1}$ and $k_{SEI2}$. Let us denote the impedance measurements in the SEI arc as

$$\begin{aligned} s_r(k) &\triangleq z_r(k) \quad \text{s.t. } k_{SEI1} \leq k \leq k_{SEI2} \\ s_i(k) &\triangleq z_i(k) \quad \text{s.t. } k_{SEI2} \leq k \leq k_{SEI2} \end{aligned} \tag{2.16}$$

where $z_r(k) = Re(Z(\omega_k))$ and $z_i(k) = Im(Z(\omega_k))$.

The estimation of $R_{\text{SEI}}$ is to fit the SEI arc using a semicircle with its centre lying on the real axis; the coordinate of this semicircle's center can be denoted as ($x_s$, 0); the radius of the semicircle can be denoted as $r_s$; thus, the measurements in (2.16) should satisfy the equation of the semicircle [22]:

$$(s_r(k) - x_s)^2 + (s_i(k) - 0)^2 = {r_s}^2 \tag{2.17}$$

$$s_r(k)^2 - 2x_s s_r(k) + x_s^2 + s_i(k)^2 = {r_s}^2 \tag{2.18}$$

Let $c = -2x_s$ and $d = x_s^2 - {r_s}^2$, thus

$${r_s}^2 = \frac{c^2}{4} - d \tag{2.19}$$

$$r_s = \sqrt{\frac{c^2}{4} - d} \tag{2.20}$$

And (2.18) can be rewritten as

$$s_r(k)^2 + s_i(k)^2 + cs_r(k) + d = 0 \tag{2.21}$$

In the matrix form, (2.21) can be written as

$$\begin{aligned} \underbrace{\begin{bmatrix} -\left(s_r(k_{SEI1})^2 + s_i(k_{SEI1})^2\right) \\ -\left(s_r(k_{SEI1}+1)^2 + s_i(k_{SEI1}+1)^2\right) \\ -\left(s_r(k_{SEI1}+2)^2 + s_i(k_{SEI1}+2)^2\right) \\ \vdots \\ -\left(s_r(k_{SEI2})^2 + s_i(k_{SEI2})^2\right) \end{bmatrix}}_{\mathbf{z}} \\ = \underbrace{\begin{bmatrix} s_r(k_{SEI1}) & 1 \\ s_r(k_{SEI1}+1) & 1 \\ s_r(k_{SEI1}+2) & 1 \\ \vdots & \\ s_r(k_{SEI2}) & 1 \end{bmatrix}}_{\mathbf{B}} \underbrace{\begin{bmatrix} c \\ d \end{bmatrix}}_{\mathbf{x}_{\text{SEI}}} + \underbrace{\begin{bmatrix} n_v(1) \\ n_v(2) \\ \vdots \\ n_v(n) \end{bmatrix}}_{\mathbf{n}} \end{aligned} \tag{2.22}$$

Using LS algorithm, the estimate of $\hat{\mathbf{x}}_{\text{SEI}}$ will be given by

$$\hat{\mathbf{x}}_{\text{SEI}} = (\mathbf{B}^T\mathbf{B})^{-1}(\mathbf{B}^T\mathbf{z}) \tag{2.23}$$

The estimates of $c$ and $d$ are:

$$\hat{c} = \hat{\mathbf{x}}_{\mathrm{SEI}}(1), \quad \hat{d} = \hat{\mathbf{x}}_{\mathrm{SEI}}(2) \tag{2.24}$$

From Fig. 2.4, $\mathrm{R_{SEI}}$ is the diameter of the SEI arc; thus, by substituting the values of $c$ and $d$ in (2.20), the estimate of $R_{\mathrm{SEI}}$ is

$$\hat{R}_{\mathrm{SEI}} = 2\hat{r}_s = 2\sqrt{\frac{\hat{c}^2}{4} - \hat{d}} \tag{2.25}$$

The estimated centre of the semicircle can then be expressed as

$$(\hat{x}_s, 0) = (-\frac{\hat{c}}{2}, 0) \tag{2.26}$$

The fitting accuracy of the SEI arc can be evaluated as [23]

$$\mathrm{RMSE_{SEI}} = \sqrt{\frac{\sum_{k=k_{SEI1}}^{k_{SEI2}} {d_k}^2}{k_{SEI2} - k_{SEI1} + 1}} \tag{2.27}$$

Where $d_k$ is the geometrical distance between the actual EIS data point and predicted EIS data point, which is defined as

$$d_k = \sqrt{[s_r(k) - \hat{x}_s]^2 + [s_i(k) - 0]^2} - \hat{r}_s \tag{2.28}$$

It can be shown in (2.1) that when the frequency is very high, the impedance in CT arc and Diffusion arc will be minimal so that it is negligible; thus, we assume the $Z_{CT\&DF}$ term will be zero, that is

$$Z = Z_{\mathrm{RL}} + Z_{\mathrm{SEI}} + 0 \tag{2.29}$$

Therefore, the impedance in SEI arc can be expressed as:

$$Z_{\mathrm{SEI}} = Z - Z_{\mathrm{RL}} \tag{2.30}$$

$$\frac{R_{\mathrm{SEI}}}{1 + j\omega R_{\mathrm{SEI}} C_{\mathrm{SEI}}} = Z(\omega) - j\omega L - R_{\Omega} \tag{2.31}$$

$$1 + j\omega R_{\mathrm{SEI}} C_{\mathrm{SEI}} = \frac{R_{\mathrm{SEI}}}{Z(\omega) - j\omega L - R_{\Omega}} \tag{2.32}$$

$$j\omega R_{\mathrm{SEI}} C_{\mathrm{SEI}} = \frac{R_{\mathrm{SEI}}}{Z(\omega) - j\omega L - R_{\Omega}} - 1 \tag{2.33}$$

$$j\omega C_{\mathrm{SEI}} = \frac{1}{Z(\omega) - j\omega L - R_{\Omega}} - \frac{1}{R_{\mathrm{SEI}}} \tag{2.34}$$

Take the imaginary part on both sides of the above equation,

$$C_{\mathrm{SEI}} = \left(\frac{1}{\omega}\right) \mathrm{Im}\left(\frac{1}{Z(\omega) - j\omega L - R_{\Omega}} - \frac{1}{R_{\mathrm{SEI}}}\right) \tag{2.35}$$

$$C_{\mathrm{SEI}} = \left(\frac{1}{\omega}\right) \mathrm{Im}\left(\frac{1}{Z(\omega) - j\omega L - R_{\Omega}}\right) \tag{2.36}$$

Substituting the expression for $R_{\Omega}$ and $L$ from (2.2) and (2.3), respectively, in (2.36) at $\omega = \omega_k$ ($k_{SEI1} \leq k \leq k_{SEI2}$):

$$\tilde{C}_{\mathrm{SEI}}(k) = \left(\frac{1}{\omega_k}\right) \mathrm{Im}\left(\frac{1}{Z(\omega_k) - j\omega_k \hat{L} - \hat{R}_{\Omega}}\right) \tag{2.37}$$

Finally, average all the estimates $\tilde{C}_{\mathrm{SEI}}(k)$ to obtain the final estimate

$$\hat{C}_{\mathrm{SEI}} = \frac{1}{k_{SEI2} - k_{SEI1} + 1} \sum_{k=k_{SEI1}}^{k_{SEI2}} \tilde{C}_{\mathrm{SEI}}(k) \tag{2.38}$$

Using the LS approach to identify $R_{SEI}$ and $C_{SEI}$ via the automatic selection of feature points are fully described in Algorithm 3. In addition, Fig. 2.7a shows the RMSE of the fitted SEI arc in each iteration and 2.7b shows the SEI arc, which is selected since it can reach the best fit. Algorithm 3 uses the following MATLAB commands: 'floor', 'length'.

**Algorithm 3** Estimate $R_{SEI}$ and $C_{SEI}$ via automatic feature detection

**Input:** $\mathbf{z}_r$, $\mathbf{z}_i$, $k_{SEI}^L$, $\hat{R}_\Omega$, $\hat{L}$
**Output:** $\hat{R}_{\text{SEI}}$, $\hat{C}_{\text{SEI}}$.

$n = 0$
$range\_SEI \leftarrow floor(length(\mathbf{z}_r)/4)$
$k_{SEI2} \leftarrow length(find(-\mathbf{z}_i \geq 0))$
**for** $k_{SEI1} = k_{SEI}^L : k_{SEI2} - range\_SEI$ **do**
    $n = n + 1$
    $\mathbf{z}_r^{fit} \leftarrow \mathbf{z}_r(k_{SEI1} : k_{SEI2})$
    $\mathbf{z}_i^{fit} \leftarrow \mathbf{z}_i(k_{SEI1} : k_{SEI2})$
    $\mathbf{kID}(n, :) \leftarrow [k_{SEI1}, k_{SEI2}]$
    $\mathbf{R}_{\text{SEI}}(n) \leftarrow$ Use $\mathbf{z}_r^{fit}$ and $\mathbf{z}_i^{fit}$ to compute $R_{\text{SEI}}$ via Eq. (2.16) - (2.25)
    $\mathbf{RMSE}(n) \leftarrow$ Compute RMSE via Eq. (2.26) - (2.28)
**end for**
$idx \leftarrow$ Find the index points to the lowest value in **RMSE**
$\hat{R}_{\text{SEI}} \leftarrow \mathbf{R}_{\text{SEI}}(idx)$
**kSEI_index** $\leftarrow \mathbf{kID}(idx, :)$ ▷ Identify the range of data points that can reach the best fit
$\hat{C}_{\text{SEI}} \leftarrow$Use the **kSEI_index** to estimate $C_{SEI}$ via Eq. (2.37) - (2.38)

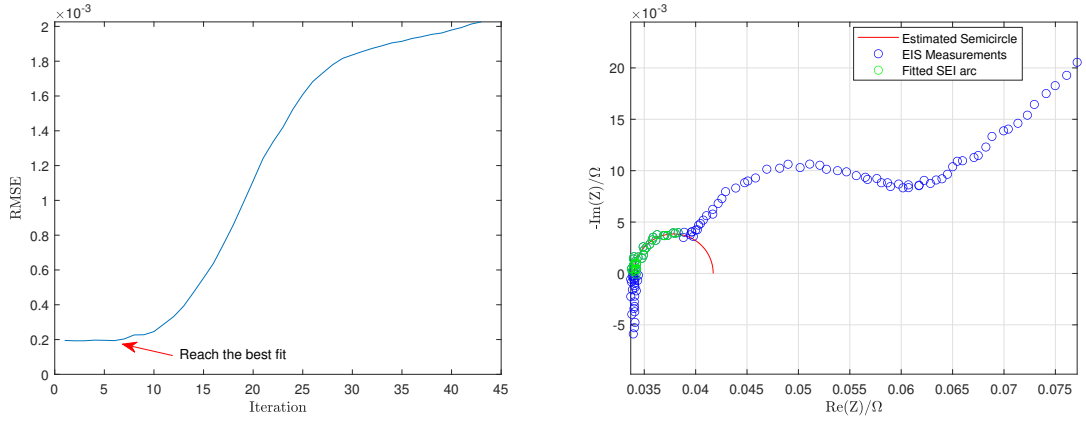


(a) (b)

Figure 2.7: **Fitted SEI arc and CT arc using LS approach.** (a) RMSE of the fitted SEI arc. (b) Best fitting of SEI arc.

### 2.3.5 Estimation of $R_{\text{CT}}$ and $C_{\text{DL}}$

It can be observed in Fig. 2.4 that to fit the CT arc using a semicircle precisely, we need to select feature points that lie between $k_{CT1}$ to $k_{CT2}$; therefore, the impedance

measurements in the CT arc can be denoted as:

$$\begin{aligned} c_r(k) &\triangleq z_r(k) \quad \text{s.t. } k_{CT1} \le k \le k_{CT2} \\ c_i(k) &\triangleq z_i(k) \quad \text{s.t. } k_{CT1} \le k \le k_{CT2} \end{aligned} \tag{2.39}$$

where $z_r(k) = Re(Z(\omega_k))$ and $z_i(k) = Im(Z(\omega_k))$.

Assuming that the centre of the semicircle lies on the real axis, which is noted as $(x_c,\ 0)$, the radius of the semicircle can be noted as $r_c$; thus, the measurements in (2.39) should satisfy the equation of the semicircle [22]:

$$(c_r(k) - x_c)^2 + (c_i(k) - 0)^2 = {r_c}^2 \tag{2.40}$$

$$c_r(k)^2 - 2x_c c_r(k) + x_c^2 + c_i(k)^2 = {r_c}^2 \tag{2.41}$$

Let $g = -2x_c$ and $h = x_c^2 - {r_c}^2$, thus

$${r_c}^2 = \frac{g^2}{4} - h \tag{2.42}$$

$$r_c = \sqrt{\frac{g^2}{4} - h} \tag{2.43}$$

And (2.41) can be rewritten as

$$c_r(k)^2 + c_i(k)^2 + g c_r(k) + h = 0 \tag{2.44}$$

In the matrix form, (2.44) can be written as

$$\underbrace{\begin{bmatrix} -\left(c_r(k_{CT1})^2 + c_i(k_{CT1})^2\right) \\ -\left(c_r(k_{CT1}+1)^2 + c_i(k_{CT1}+1)^2\right) \\ -\left(c_r(k_{CT1}+2)^2 + c_i(k_{CT1}+2)^2\right) \\ \vdots \\ -\left(c_r(k_{CT2})^2 + c_i(k_{CT2})^2\right) \end{bmatrix}}_{\mathbf{p}} = \underbrace{\begin{bmatrix} c_r(k_{CT1}) & 1 \\ c_r(k_{CT1}+1) & 1 \\ c_r(k_{CT1}+2) & 1 \\ \vdots & \\ c_r(k_{CT2}) & 1 \end{bmatrix}}_{\mathbf{C}} \underbrace{\begin{bmatrix} g \\ h \end{bmatrix}}_{\mathbf{x}_{\mathrm{CT}}} + \underbrace{\begin{bmatrix} n_v(1) \\ n_v(2) \\ \vdots \\ n_v(n) \end{bmatrix}}_{\mathbf{n}} \tag{2.45}$$

From (2.45), $\mathbf{x}_{\mathrm{CT}}$ can be estimated using LS algorithm

$$\hat{\mathbf{x}}_{\mathrm{CT}} = (\mathbf{C}^T\mathbf{C})^{-1}(\mathbf{C}^T\mathbf{p}) \tag{2.46}$$

Thus, the estimates of $a$ and $b$ are:

$$\hat{g} = \hat{\mathbf{x}}_{\mathrm{CT}}(1), \quad \hat{h} = \hat{\mathbf{x}}_{\mathrm{CT}}(2) \tag{2.47}$$

As shown in Fig. 2.4, $R_{\mathrm{CT}}$ is the diameter of the CT arc; thus, by substituting the values of $a$ and $b$ in (2.43), the estimate of $R_{\mathrm{CT}}$ is

$$\hat{R}_{\mathrm{CT}} = 2\hat{r}_c = 2\sqrt{\frac{\hat{g}^2}{4} - \hat{h}} \tag{2.48}$$

The estimated centre of the semicircle can then be expressed as

$$(\hat{x}_c, 0) = (-\frac{\hat{g}}{2}, 0) \tag{2.49}$$

The fitting accuracy of the CT arc can be evaluated as [23]

$$\mathrm{RMSE_{CT}} = \sqrt{\frac{\sum_{k=k_{CT1}}^{k_{CT2}} {d_k}^2}{k_{CT2} - k_{CT1} + 1}} \tag{2.50}$$

Where $d_k$ is the geometrical distance between the actual EIS data point and predicted EIS data point, which is defined as [23]

$$d_k = \sqrt{[c_r(k) - \hat{x}_c]^2 + [c_i(k) - 0]^2} - \hat{r}_c \tag{2.51}$$

Based on (2.1),

$$Z = Z_{\mathrm{RL}} + Z_{\mathrm{SEI}} + Z_{\mathrm{CT\&DF}} \tag{2.52}$$

Therefore, the impedance in CT arc and DF arc can be expressed as:

$$Z_{\mathrm{CT\&DF}} = Z - Z_{\mathrm{RL}} - Z_{\mathrm{SEI}} \tag{2.53}$$

$$\begin{aligned} &\frac{R_{\mathrm{CT}} + Z_{\mathrm{w}}(j\omega)}{1 + j\omega \left(R_{\mathrm{CT}} + Z_{\mathrm{w}}(j\omega)\right) C_{\mathrm{DL}}} \\ &= Z(\omega) - j\omega L - R_\Omega - \frac{R_{\mathrm{SEI}}}{1 + j\omega R_{\mathrm{SEI}} C_{\mathrm{SEI}}} \end{aligned} \tag{2.54}$$

Thus,

$$\begin{aligned} &j\omega \left(R_{\mathrm{CT}} + Z_{\mathrm{w}}(j\omega)\right) C_{\mathrm{DL}} \\ &= \frac{R_{\mathrm{CT}} + Z_{\mathrm{w}}(j\omega)}{Z(\omega) - j\omega L - R_\Omega - \frac{R_{\mathrm{SEI}}}{1 + j\omega R_{\mathrm{SEI}} C_{\mathrm{SEI}}}} - 1 \end{aligned} \tag{2.55}$$

Then,

$$j\omega C_{\mathrm{DL}} = \frac{1}{Z(\omega) - j\omega L - R_{\Omega} - \frac{R_{\mathrm{SEI}}}{1+j\omega R_{\mathrm{SEI}} C_{\mathrm{SEI}}}} - \frac{1}{R_{\mathrm{CT}} + Z_{\mathrm{w}}(j\omega)} \tag{2.56}$$

Take the imaginary part on both sides of (2.56), and substitute $Z_w(jw)$ with the expression given in (2.13), we obtain

$$\begin{aligned} & C_{\mathrm{DL}} \\ &= \left(\frac{1}{\omega}\right) \mathrm{Im} \left( \frac{1}{Z(\omega) - j\omega L - R_{\Omega} - \frac{R_{\mathrm{SEI}}}{1+j\omega R_{\mathrm{SEI}} C_{\mathrm{SEI}}}} \right. \\ & \left. - \frac{1}{R_{\mathrm{CT}} + (1 - jm)\frac{\sigma}{\sqrt{\omega}}} \right) \end{aligned} \tag{2.57}$$

Substituting $L$, $R_{\Omega}$, $R_{\mathrm{SEI}}$, $C_{\mathrm{SEI}}$, $R_{\mathrm{CT}}$ and $\sigma$ with the estimations given in (2.3), (2.2), (2.25), (2.38), (2.48) and (2.15) respectively, in the above equation at $\omega = \omega_k$ ($k_{CT1} \leq k \leq k_{CT2}$):

$$\begin{aligned} & \tilde{C}_{\mathrm{DL}}(k) \\ &= \left(\frac{1}{\omega_k}\right) \mathrm{Im} \left( \frac{1}{Z(\omega_k) - j\omega_k \hat{L} - \hat{R}_{\Omega} - \frac{\hat{R}_{\mathrm{SEI}}}{1+j\omega_k \hat{R}_{\mathrm{SEI}} \hat{C}_{\mathrm{SEI}}}} \right. \\ & \left. - \frac{1}{\hat{R}_{\mathrm{CT}} + (1 - j\hat{m})\frac{\hat{\sigma}}{\sqrt{\omega_k}}} \right) \end{aligned} \tag{2.58}$$

Finally, average all the estimates $\tilde{C}_{\mathrm{DL}}(k)$ to obtain the final estimate

$$\hat{C}_{\mathrm{DL}} = \frac{1}{k_{CT2} - k_{CT1} + 1} \sum_{k=k_{CT1}}^{k_{CT2}} \tilde{C}_{\mathrm{DL}}(k) \tag{2.59}$$

Using the LS approach to identify $R_{CT}$ and $C_{DL}$ via the automatic selection of feature points is shown in Algorithm 4. Furthermore, Fig. 2.8a shows the RMSE of the fitted CT arc in each iteration, and 2.8b shows the CT arc selected since it can

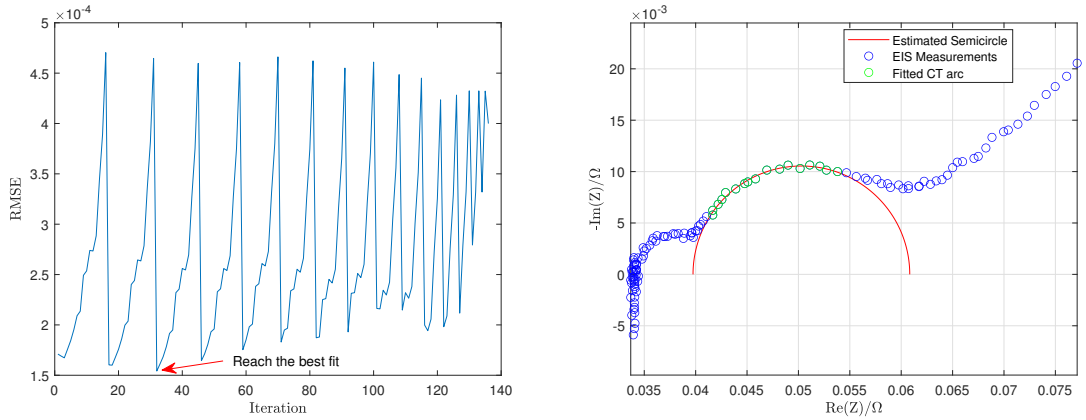


(a) (b)

Figure 2.8: **Fitted SEI arc and CT arc using LS approach.** (a) RMSE of the fitted CT arc. (b) Best fitting of CT arc.

reach the best fit. Algorithm 4 uses the following MATLAB commands: 'floor' and 'round'.

**Algorithm 4** Estimate $R_{CT}$ and $C_{DL}$ via automatic feature detection

**Input:** $\mathbf{z}_r$, $\mathbf{z}_i$, $k_{CT}^L$, $k_{SEI2}$, $\hat{R}_\Omega$, $\hat{L}$, $\hat{R}_{\text{SEI}}$, $\hat{C}_{\text{SEI}}$, $\hat{\sigma}_{LS}$, $\hat{m}$
**Output:** $\hat{R}_{\text{CT}}$, $\hat{C}_{\text{DL}}$,

$n = 0$
$k_{CT}^U \leftarrow k_{SEI2} - floor((k_{SEI2} - k_{CT}^L)/2)$ ▷ the uppermost bound of the CT arc
$range_{CT} \leftarrow round((k_{CT}^U - k_{CT}^L)/2)$
**for** $k_{CT1} = k_{CT}^L : (k_{CT}^U - range_{CT})$ **do**
    **for** $k_{CT2} = (k_{CT}^L + range_{CT}) : k_{CT}^U$ **do**
        $n = n + 1$
        $\mathbf{z}_r^{fit} \leftarrow \mathbf{z}_r(k_{CT1} : k_{CT2})$
        $\mathbf{z}_i^{fit} \leftarrow \mathbf{z}_i(k_{CT1} : k_{CT2})$
        $\mathbf{kID}(n, :) = [k_{CT1}, k_{CT2}]$
        $\mathbf{R}_{\text{CT}}(n) \leftarrow$ Use $\mathbf{z}_r^{fit}$ and $\mathbf{z}_i^{fit}$ to compute $R_{\text{CT}}$ via Eq. (2.39) - (2.48)
        $\mathbf{RMSE}(n) \leftarrow$ Compute RMSE via Eq. (2.49) - (2.51)
    **end for**
**end for**
$idx \leftarrow$ Find the index points to the lowest value in **RMSE**
$\hat{R}_{\text{CT}} \leftarrow \mathbf{R}_{\text{CT}}(idx)$
**kCT_index** = $\mathbf{kID}(idx, :)$ ▷ the range of data points that can reach the best fit
$\hat{C}_{\text{DL}} \leftarrow$Use the **kCT_index** to estimate $C_{\text{DL}}$ via Eq. (2.58) - (2.59)

### 2.3.6 Evaluation of the General Fitting Accuracy

In the complex plane, the absolute value of the error between the measured EIS and estimated EIS is actually the distance between measured EIS data points and estimated EIS data points as shown in Fig.2.9, $d_1$, where $d_2$, ... $d_n$ are the distances between measured EIS data point $(z_r(k), z_i(k))$ and estimated EIS data point $(\hat{z}_r(k), \hat{z}_i(k))$, which can be used to evaluate the fitting accuracy, the distance $d_k$ is represented as.

$$d_k = \sqrt{[z_r(k) - \hat{z}_r(k)]^2 + [z_i(k) - \hat{z}_i(k)]^2} \tag{2.60}$$

Where $n$ is the number of measurements, $k \in 1, 2, ..., n$.

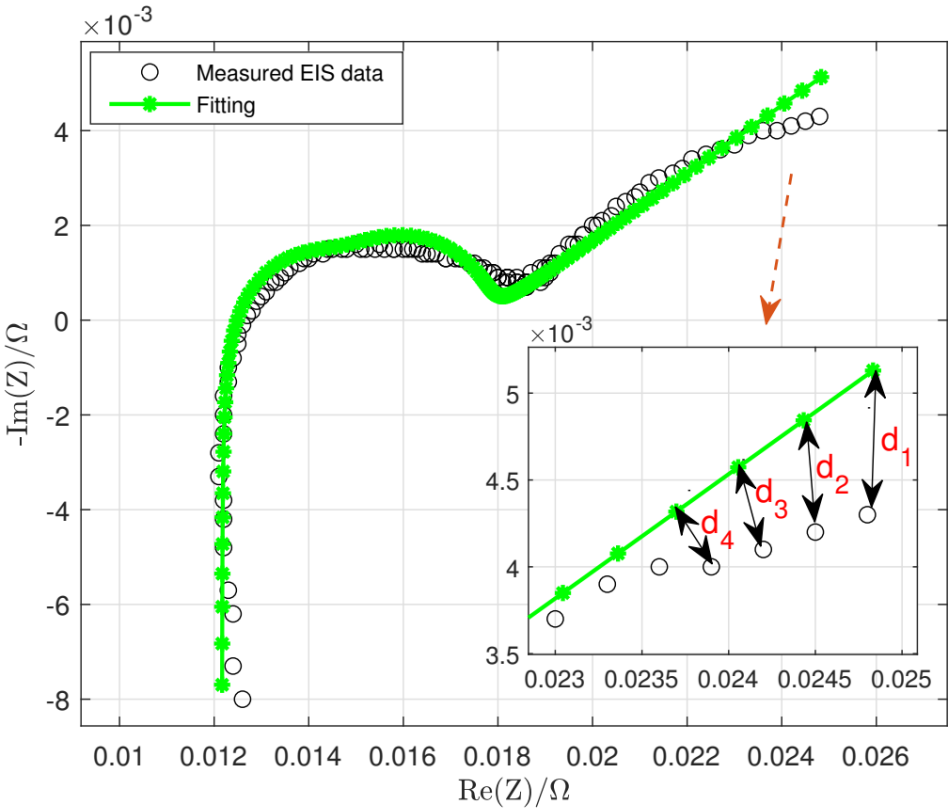


Figure 2.9: **Geometrical distance between measured EIS data point and predicted EIS data point.**

Therefore, the evaluation of EIS fitting can be expressed as

$$\text{MAE} = \frac{1}{N}\sum_{k=1}^{N} d_k = \frac{1}{N}\sum_{k=1}^{N}\left|Z(\omega_k) - \hat{Z}(\omega_k)\right| \tag{2.61}$$

Where $Z(\omega_k)$ is the measured impedance at $\omega_k$, $\hat{Z}(\omega_k)$ is the impedance estimation at $\omega_k$, which is computed based on (2.1) with the estimated ECM parameters, $N$ is the total number of measurements, $|\cdot|$ denotes the absolute value of the complex number.

The goal is to fit the EIS measurements such that the fitted EIS can achieve the lowest MAE.

The percentage error of the estimated parameters can be expressed as:

$$\begin{aligned}&\text{Percentage Error (\%)}\\ &= \left|\frac{\text{True Value} - \text{Predicted Value}}{\text{True Value}}\right| \times 100\%\end{aligned} \tag{2.62}$$

## 2.4 Exhaustive Search Approach

### 2.4.1 Second Estimation of Warburg Coefficient $\sigma$

Assume $R_\Omega$, $L$, $R_{SEI}$, $C_{SEI}$, $R_{CT}$, $C_{DL}$ and $m$ are given, based on (2.54),

$$\begin{aligned}&\frac{1}{\frac{1}{R_{\text{CT}}+Z_{\text{w}}(j\omega)} + j\omega C_{\text{DL}}}\\ &= Z(\omega) - j\omega L - R_\Omega - \frac{R_{\text{SEI}}}{1 + j\omega R_{\text{SEI}} C_{\text{SEI}}}\end{aligned} \tag{2.63}$$

$$\begin{aligned}&\frac{1}{R_{\text{CT}} + Z_{\text{w}}(j\omega)} + j\omega C_{\text{DL}}\\ &= \frac{1}{Z(\omega) - j\omega L - R_\Omega - \frac{R_{\text{SEI}}}{1+j\omega R_{\text{SEI}} C_{\text{SEI}}}}\end{aligned} \tag{2.64}$$

thus,

$$\begin{aligned}&\frac{1}{R_{\mathrm{CT}}+Z_{\mathrm{w}}(j\omega)}\\&=\frac{1}{Z(\omega)-j\omega L-R_{\Omega}-\frac{R_{\mathrm{SEI}}}{1+j\omega R_{\mathrm{SEI}}C_{\mathrm{SEI}}}}-j\omega C_{\mathrm{DL}}\end{aligned}\tag{2.65}$$

$$\begin{aligned}&R_{\mathrm{CT}}+Z_{\mathrm{w}}(j\omega)\\&=\frac{1}{\frac{1}{Z(\omega)-j\omega L-R_{\Omega}-\frac{R_{\mathrm{SEI}}}{1+j\omega R_{\mathrm{SEI}}C_{\mathrm{SEI}}}}-j\omega C_{\mathrm{DL}}}\end{aligned}\tag{2.66}$$

then, the Warburg impedance can also be expressed as:

$$\begin{aligned}&Z_{\mathrm{w}}(j\omega)\\&=\frac{1}{\frac{1}{Z(\omega)-j\omega L-R_{\Omega}-\frac{R_{\mathrm{SEI}}}{1+j\omega R_{\mathrm{SEI}}C_{\mathrm{SEI}}}}-j\omega C_{\mathrm{DL}}}-R_{\mathrm{CT}}\end{aligned}\tag{2.67}$$

Take the real part on both sides of the above equation, at $\omega=\omega_k$ ($k_{DF1}\leq k\leq k_{DF2}$),

$$\begin{aligned}&\mathrm{Re}\left(Z_{\mathrm{w}}(j\omega_k)\right)\\&=\mathrm{Re}\left(\frac{1}{\frac{1}{Z(\omega_k)-j\omega_k L-R_{\Omega}-\frac{R_{\mathrm{SEI}}}{1+j\omega_k R_{\mathrm{SEI}}C_{\mathrm{SEI}}}}-j\omega_k C_{\mathrm{DL}}}-R_{\mathrm{CT}}\right)\end{aligned}\tag{2.68}$$

The real part of the Warburg impedance can be noted as:

$$W_r(k)\triangleq\mathrm{Re}\left(Z_{\mathrm{w}}(j\omega_k)\right)\qquad\text{s.t. } k_{DF1}\leq k\leq k_{DF2}\tag{2.69}$$

Take the real part on both sides of (2.12), we get

$$W_r(k)=\frac{\sigma}{\sqrt{\omega_k}}\tag{2.70}$$

Thus,

$$\tilde{\sigma}_k^{ES}=W_r(k)\sqrt{\omega_k}\tag{2.71}$$

Finally, average all the estimates $\tilde{\sigma}_k^{ES}$ to obtain the final estimate

$$\hat{\sigma}_{ES} = \frac{1}{k_{DF2} - k_{DF1} + 1} \sum_{k=k_{DF1}}^{k_{DF2}} \tilde{\sigma}_k^{ES} \tag{2.72}$$

### 2.4.2 Specify the Range of Parameters for Exhaustive Search

As presented in section 2.3, the rough estimations of ECM parameters are given; therefore, we can assign the lower and upper bound for each parameter such that the exhaustive search approach can identify the most suitable parameter between the boundary. As shown in Algorithm 5, the range of each ECM parameter is assigned based on the empirical coefficient. In this chapter, the size of possible values in each ECM parameter is restricted to 20 such that the computational time is within the acceptable range. Algorithm 5 uses the MATLAB command 'linspace'.

**Algorithm 5** Set the range of ECM parameters estimated by LS approach .

**Input:** $\hat{R}_{\text{SEI}}$, $\hat{C}_{\text{SEI}}$, $\hat{R}_{\text{CT}}$, $\hat{C}_{\text{DL}}$, $\hat{m}$
**Output:** $\{R_{\text{SEI}}^{min}, \ldots, R_{\text{SEI}}^{max}\}$, $\{C_{\text{SEI}}^{min}, \ldots, C_{\text{SEI}}^{max}\}$, $\{R_{\text{CT}}^{min}, \ldots, R_{\text{CT}}^{max}\}$, $\{C_{\text{DL}}^{min}, \ldots, C_{\text{DL}}^{max}\}$, $\{m^{min}, \ldots, m^{max}\}$

1: $\{R_{\text{SEI}}^{min}, \ldots, R_{\text{SEI}}^{max}\} \leftarrow linspace(0.2\hat{R}_{\text{SEI}}, 2\hat{R}_{\text{SEI}}, 20)$
2: $\{C_{\text{SEI}}^{min}, \ldots, C_{\text{SEI}}^{max}\} \leftarrow linspace(\hat{C}_{\text{SEI}}, 2.5\hat{C}_{\text{SEI}}, 20)$
3: $\{R_{\text{CT}}^{min}, \ldots, R_{\text{CT}}^{max}\} \leftarrow linspace(0.5\hat{R}_{\text{CT}}, 1.5\hat{R}_{\text{CT}}, 20)$
4: $\{C_{\text{DL}}^{min}, \ldots, C_{\text{DL}}^{max}\} \leftarrow linspace(\hat{C}_{\text{DL}}, 3\hat{C}_{\text{DL}}, 20)$
5: $\{m^{min}, \ldots, m^{max}\} \leftarrow linspace(0.8\hat{m}, 1.2\hat{m}, 20)$

### 2.4.3 Implement Exhaustive Search

Algorithm 6 describes the ES approach that can be applied to precisely identify the ECM parameters, which are roughly estimated in the previous section. Fig. 2.10 shows the MAE evaluated from the initial iteration throughout the end of the exhaustive search process; by finding the lowest MAE in this figure, one can identify the best estimation of ECM parameters via the ES approach.

**Algorithm 6** Exhaustive Search Approach.

**Input:** $\{R_{\text{SEI}}^{min}, \ldots, R_{\text{SEI}}^{max}\}$, $\{C_{\text{SEI}}^{min}, \ldots, C_{\text{SEI}}^{max}\}$, $\{R_{\text{CT}}^{min}, \ldots, R_{\text{CT}}^{max}\}$, $\{C_{\text{DL}}^{min}, \ldots, C_{\text{DL}}^{max}\}$, $\{m^{min}, \ldots, m^{max}\}$, $\hat{R}_{\Omega}$, $\hat{L}$
**Output:** $\text{MAE}_{\text{min}}^{\text{ES}}$, $\mathbf{P}_{\text{ES}}$

$n = 0$
**for** $R_{\text{SEI}} \in \{R_{\text{SEI}}^{min}, \ldots, R_{\text{SEI}}^{max}\}$ **do**
    **for** $C_{\text{SEI}} \in \{C_{\text{SEI}}^{min}, \ldots, C_{\text{SEI}}^{max}\}$ **do**
        **for** $R_{\text{CT}} \in \{R_{\text{CT}}^{min}, \ldots, R_{\text{CT}}^{max}\}$ **do**
            **for** $C_{\text{DL}} \in \{C_{\text{DL}}^{min}, \ldots, C_{\text{DL}}^{max}\}$ **do**
                **for** $m \in \{m^{min}, \ldots, m^{max}\}$ **do**
                    $n = n + 1$
                    Second Estimation of $\sigma$ using Eq. (2.68) to (2.72)
                    Use the estimated ECM parameters in each iteration to generate simulated EIS data
                    Compute $\mathbf{MAE}(n)$ using Eq. (2.61)
                **end for**
            **end for**
        **end for**
    **end for**
**end for**
$\text{MAE}_{\text{min}}^{\text{ES}} \leftarrow$ Find the lowest value of **MAE**
$idx \leftarrow$ Find the index of $\text{MAE}_{\text{min}}$ in **MAE**
$\mathbf{P}_{\text{ES}} \leftarrow$ Identify the ECM parameters using the index $idx$ that points to the lowest MAE
Compute percentage error (In EIS simulation test procedure)

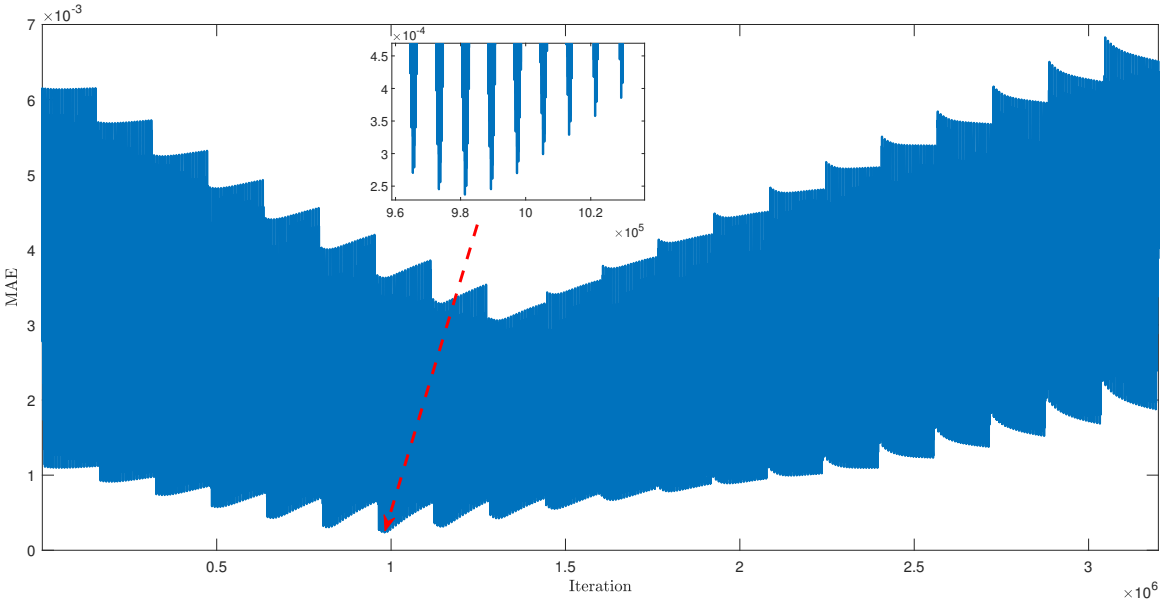


Figure 2.10: **Find the lowest MAE of ES approach.**

## 2.5 Nonlinear Least Squares Approach

The concept of implementing the NLS approach based on the Monte-Carlo run is shown in Fig. 2.11. This approach randomly selects initial guesses of the ECM parameters in each Monte Carlo run to fit the EIS data in different cases.

### 2.5.1 Objective function

The goal is to find the optimized ECM parameters to minimize the following function.

$$\hat{\mathbf{x}} = \arg\min_{\mathbf{x}} \sum_{k=1}^{N} |\hat{Z}(\omega_k) - Z(\omega_k)| \tag{2.73}$$

Where,

$$\mathbf{x} = [R_\Omega, L, R_{SEI}, C_{SEI}, R_{CT}, C_{DL}, \sigma, m] \tag{2.74}$$

$$\hat{Z}(\omega_k) = \hat{\mathbf{x}}(1) + j\omega_k\hat{\mathbf{x}}(2) + \frac{1}{\frac{1}{\hat{\mathbf{x}}(3)} + j\omega_k\hat{\mathbf{x}}(4)} + \frac{1}{\frac{1}{\hat{\mathbf{x}}(5)+(1-j\hat{\mathbf{x}}(8))\frac{\hat{\mathbf{x}}(7)}{\sqrt{\omega_k}}} + j\omega\hat{\mathbf{x}}(6)} \tag{2.75}$$

and $Z(\omega_k)$ is the measured impedance at $\omega_k$, $N$ is total number of measurements, $|\cdot|$ denotes the absolute value of the complex number.

The nonlinear least square approach is implemented in MATLAB using the built-in function *lsqnonlin* to fit the EIS data.

### 2.5.2 Initial Guess

Instead of setting the lower bound and upper bound for the NLS approach, in this chapter, we randomly select the initial guess in each Monte-Carlo run to try different NLS fitting based on different initial guess; this way, to find the best fit among all cases. In MATLAB the initial guess is defined as:

$$\mathbf{x_0} = [\mathbf{abs}(\mathbf{randn}(\mathbf{1}, \mathbf{7})), \mathbf{1}] \tag{2.76}$$

### 2.5.3 Algorithm Switch

To reach the best fit, firstly, the NLS approach will apply 'trust-region-reflective' algorithm [24, 25], then the NLS approach will switch to 'levenberg-margquardt' algorithm [26–28]; since, in some cases, the curvature of the objective function can be negative; as compared to using the Levenberg-Marquardt algorithm, using the Trust Region method can reach better performance [29]. After that, the algorithm that can achieve the lowest mean absolute error (MAE) will be selected as the approach that can reach the best fit. The detailed approach is shown in Algorithm 7. This algorithm uses the following MATLAB commands: 'abs' and 'randn'.

**Algorithm 7** NLS Approach.

**Input:** measured impedance $\mathbf{Z}$
**Output:** $\mathrm{MAE}_{\mathrm{min}}^{\mathrm{NLS}}$, $\mathbf{P}_{\mathrm{NLS}}$

Define objective function
$n = 0$
**while** n $\leq 100$ **do**
    $\mathbf{x}_0 = [abs(randn(1, 7)), 1]$ ▷ Randomly set initial guess
    Solver switches to 'trust-region-reflective' algorithm
    Solver switches to 'levenberg-marquardt' algorithm
    Compute MAE
    $n = n + 1$
**end while**
Find the lowest MAE computed by 'trust-region-reflective' algorithm, denote as $\mathrm{MAE}_{\mathrm{min}}^{trf}$
Find the lowest MAE computed by 'levenberg-marquardt' algorithm, denote as $\mathrm{MAE}_{\mathrm{min}}^{lvbm}$
**if** $\mathrm{MAE}_{\mathrm{min}}^{trf} \leq \mathrm{MAE}_{\mathrm{min}}^{lvbm}$ **then**
    $\mathrm{MAE}_{\mathrm{min}}^{\mathrm{NLS}} = \mathrm{MAE}_{\mathrm{min}}^{trf}$
**else**
    $\mathrm{MAE}_{\mathrm{min}}^{\mathrm{NLS}} = \mathrm{MAE}_{\mathrm{min}}^{lvbm}$
**end if**
$\mathbf{P}_{\mathrm{NLS}} \leftarrow$ Identify the ECM parameters using the index points to the lowest MAE
Compute Percentage Error (In EIS simulation data validation procedure)

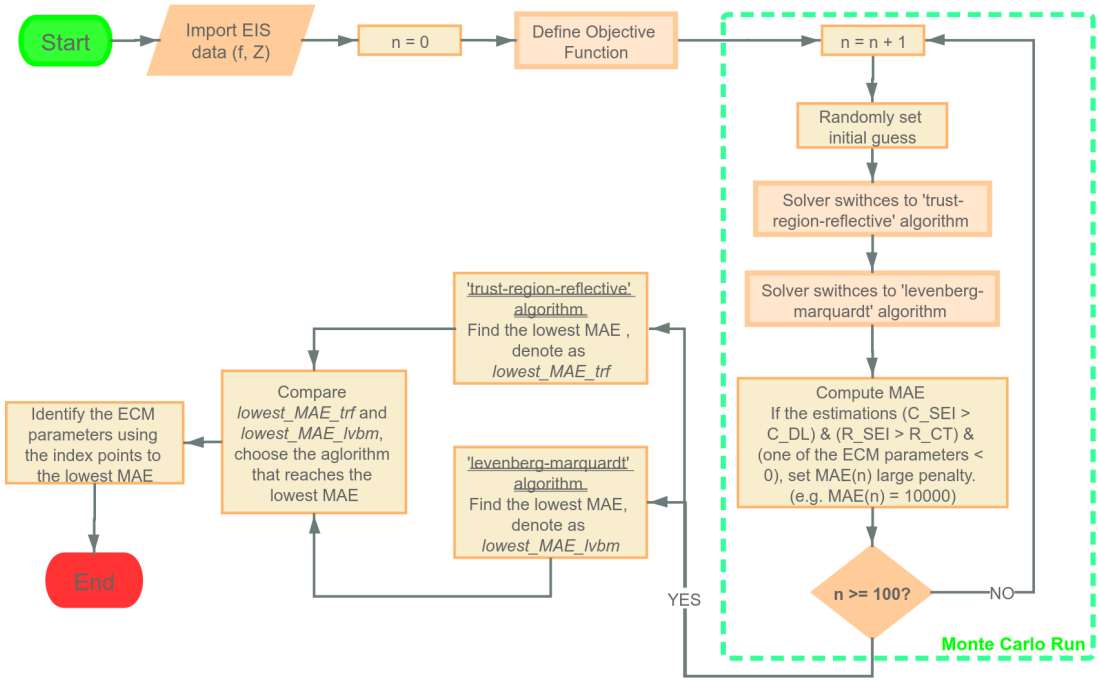


Figure 2.11: **Monte-Carlo based Nonlinear Least Sqaures Approach.**

## 2.6 Implementation

In this chapter, we implemented three ECM parameter estimation approaches in MATLAB R2020a with a 3 GHz Processor and 16 GB RAM.

### 2.6.1 Simulate EIS data

The simulated EIS data was generated using Algorithm 8, where the frequency ranges from 0.01 Hz to 10 kHz, and the number of EIS measurements is 121; this is because we want to keep the conformity with the sampling size set in the EIS experiment conducted in [22]. Table 2.1 shows the true ECM parameters for simulating EIS data. Algorithm 8 uses the MATLAB command 'linspace'.

The signal-to-noise ratio (SNR) is defined as [32]:

$$\mathrm{SNR}(dB) = 10\log_{10}\left(\frac{P_{\mathrm{signal}}}{P_{\mathrm{noise}}}\right) = 20\log_{10}\left(\frac{A_{\mathrm{signal}}}{A_{\mathrm{noise}}}\right) \tag{2.77}$$

**Algorithm 8** EIS simulation.

**Input:** $f_L$, $f_H$, $n$
**P**: True ECM paramters, $8 \times 1$ vector
**Output:** $\mathbf{z}_r$, $\mathbf{z}_i$, $\mathbf{f}$: Frequencies range from the lowest to the highest

1: $\mathbf{q} = linspace(log_{10}f_L, log_{10}f_H, n)$
2: $f_i = 10^{\mathbf{q}(\mathrm{i})}$, $i \in 1, 2, ..., n$
3: $\mathbf{f} = [f_1, f_2, ..., f_n]^{\mathrm{T}}$
4: $\omega = 2\pi\mathbf{f}$ ▷ Angular frequency, $n \times 1$ vector
5: $\mathbf{Z} \leftarrow$ Compute impedance via Eq. (2.1) based on the given ECM parameters $\mathbf{P}$ ▷ Where, $\mathbf{P} = [R_\Omega, L, R_{SEI}, C_{SEI}, R_{CT}, C_{DL}, \sigma, m]^{\mathrm{T}}$
6: $\mathbf{z}_r \leftarrow real(\mathbf{Z})$
7: $\mathbf{z}_i \leftarrow -imag(\mathbf{Z})$

Table 2.1: True ECM parameters used for EIS simulation

| $\mathbf{R_\Omega}$ (m$\Omega$) | L ($nH$) | $\mathbf{R_{SEI}}$ (m$\Omega$) | $\mathbf{C_{SEI}}$ ($F$) | $\mathbf{R_{CT}}$(m$\Omega$) | $\mathbf{C_{DL}}$ ($F$) | $\boldsymbol{\sigma}$ ($\times\mathbf{10^{-3}}$) | m |
|---|---|---|---|---|---|---|---|
| 34 | 95 | 6 | 1 | 18 | 8 | 5 | 1 |

Where $P$ is the average power, A is the root mean square (RMS) amplitude.

In this chapter, we imposed Gaussian noise on the simulated EIS data. Assume the standard deviation is $\sigma_{noise}$, the amplitude of the signal is $R_\Omega$, if SNR (dB) is given, then the $\sigma_{noise}$ can be defined as

$$\sigma_{\text{noise}} = \frac{R_\Omega}{10^{\frac{\text{SNR}}{20}}} \tag{2.78}$$

### 2.6.2 Collect Real EIS data

The impedance data is measured from two Li-ion batteries: LG 18650 and Molicel 21700. In addition, the specifications of LG and Molicel batteries are shown in [22, Tab. 1]. The data are collected using the Arbin battery cycler (Model: LBT21084UC), which has 16 channels that can operate in parallel. In this experiment, eight channels were used to collect data simultaneously at room temperature (23 °C).

As shown in Fig. 2.12, the EIS data are measured by the EIS device (Gamry

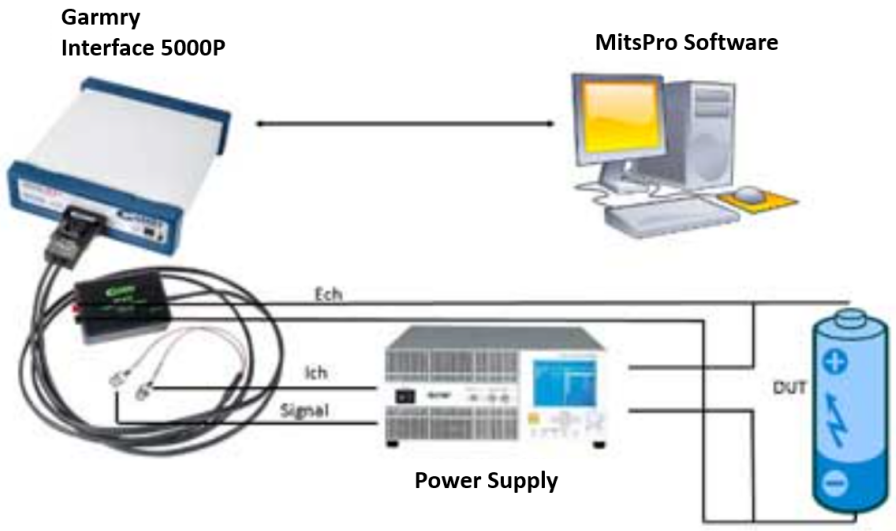


Figure 2.12: **Experimental Setup [31].**

interface 5000P). We operated the Gamry EIS device and Arbin battery cycler using the software *MitsPro* provided by Arbin company. The voltage measurement error of the Gamry EIS device is 0.2 mV as specified from [30]. In this chapter, we validated LS, ES, and NLS approaches on EIS data collected from one LG and one Molicel battery when the SOC is at 90%, 50% and 10%, while discharging from a fully charged state.

## 2.7 Results

In this section, fitting results obtained from the simulated and real EIS data are shown and discussed.

### 2.7.1 Estimation Results of ECM Parameters Using Simulated EIS Data

The comparisons of simulated EIS data fitted by LS, ES, and NLS approaches are shown in Fig. 2.13a to Fig. 2.13d. It can be observed that the LS approach shows

Table 2.2: Estimated ECM parameters, computational time, and accuracy of using LS, ES and NLS approaches to fit simulated EIS data

| **SNR** (dB) | **Approach** | $\mathbf{R_\Omega}$ (mΩ) | **L** (nH) | $\mathbf{R_{SEI}}$ (mΩ) | $\mathbf{C_{SEI}}$ (F) | $\mathbf{R_{CT}}$ (mΩ) | $\mathbf{C_{DL}}$ (F) | $\boldsymbol{\sigma}$ ($\times 10^{-3}$) | **m** | **Runtime** (sec) | **MAE** ($\times 10^{-4}$) |
|---|---|---|---|---|---|---|---|---|---|---|---|
| 35 | LS | 34.1732 | 90.0059 | 6.5913 | 0.7001 | 20.2695 | 3.7199 | 5.9541 | 0.7955 | 0.8179 | 36 |
| | ES | 34.1732 | 90.0059 | 5.6893 | 1.0318 | 17.6020 | 7.6356 | 5.1542 | 0.9546 | 132.5195 | 7.7635 |
| | NLS | 34.1513 | 94.9926 | 5.8394 | 0.9940 | 17.9632 | 7.9505 | 4.9704 | 1.0083 | 2.4578 | 7.5761 |
| 40 | LS | 33.9115 | 89.3443 | 7.9729 | 0.8487 | 21.0450 | 4.4013 | 5.6291 | 0.8273 | 1.3832 | 37 |
| | ES | 33.9115 | 89.3443 | 6.1266 | 0.9827 | 17.7220 | 8.1076 | 5.1341 | 0.9754 | 150.6105 | 4.3921 |
| | NLS | 33.9639 | 91.2816 | 5.9986 | 0.9877 | 18.0590 | 7.9177 | 4.9947 | 1.0035 | 2.4566 | 4.2861 |
| 45 | LS | 34.0076 | 93.6538 | 7.6838 | 0.8704 | 21.0861 | 4.7606 | 5.0606 | 1.0132 | 0.8481 | 31 |
| | ES | 34.0076 | 93.6538 | 5.9044 | 1.0078 | 18.3116 | 7.7674 | 4.9456 | 1.0025 | 133.6487 | 2.5021 |
| | NLS | 34.0100 | 96.2899 | 5.8936 | 1.0074 | 17.9556 | 7.8518 | 5.0690 | 0.9891 | 2.0977 | 2.2978 |
| 50 | LS | 33.9983 | 93.1031 | 7.6353 | 0.9300 | 20.8236 | 4.6782 | 5.4055 | 0.8688 | 0.7761 | 32 |
| | ES | 33.9983 | 93.1031 | 5.8671 | 1.0034 | 18.0840 | 7.6328 | 4.9885 | 1.0060 | 134.4532 | 1.6276 |
| | NLS | 33.9979 | 93.9546 | 5.9664 | 1.0366 | 17.9481 | 7.9246 | 5.0128 | 0.9960 | 2.0583 | 1.3904 |

insufficient goodness of fitting, whereas ES and NLS approaches generally reach considerable goodness of fitting. Table 2.2 shows that at any SNR, the computational time of the LS approach is the fastest; however, the fitting accuracy MAE is the lowest. On the contrary, the ES approach has the slowest computational time, but the fitting accuracy is significantly improved compared with the LS approach. The NLS approach reaches the lowest MAE and considerably faster computational time, which only takes around two seconds to complete the EIS fitting. Furthermore, with the SNR increasing, the MAE decreases.

As shown in Fig. 2.14a to Fig. 2.14d, it is clear that at any SNR, the percentage error of the estimated RC components reaches the highest when using the LS approach and reaches the lowest when using NLS approach, except for that the percentage error of $C_{SEI}$ estimated at 50 dB is higher than that when using NLS approach; besides, at any SNR, the percentage errors of estimated ECM parameters using NLS approach are well below 5% showing significantly higher estimation accuracy compared with ES and LS approaches.

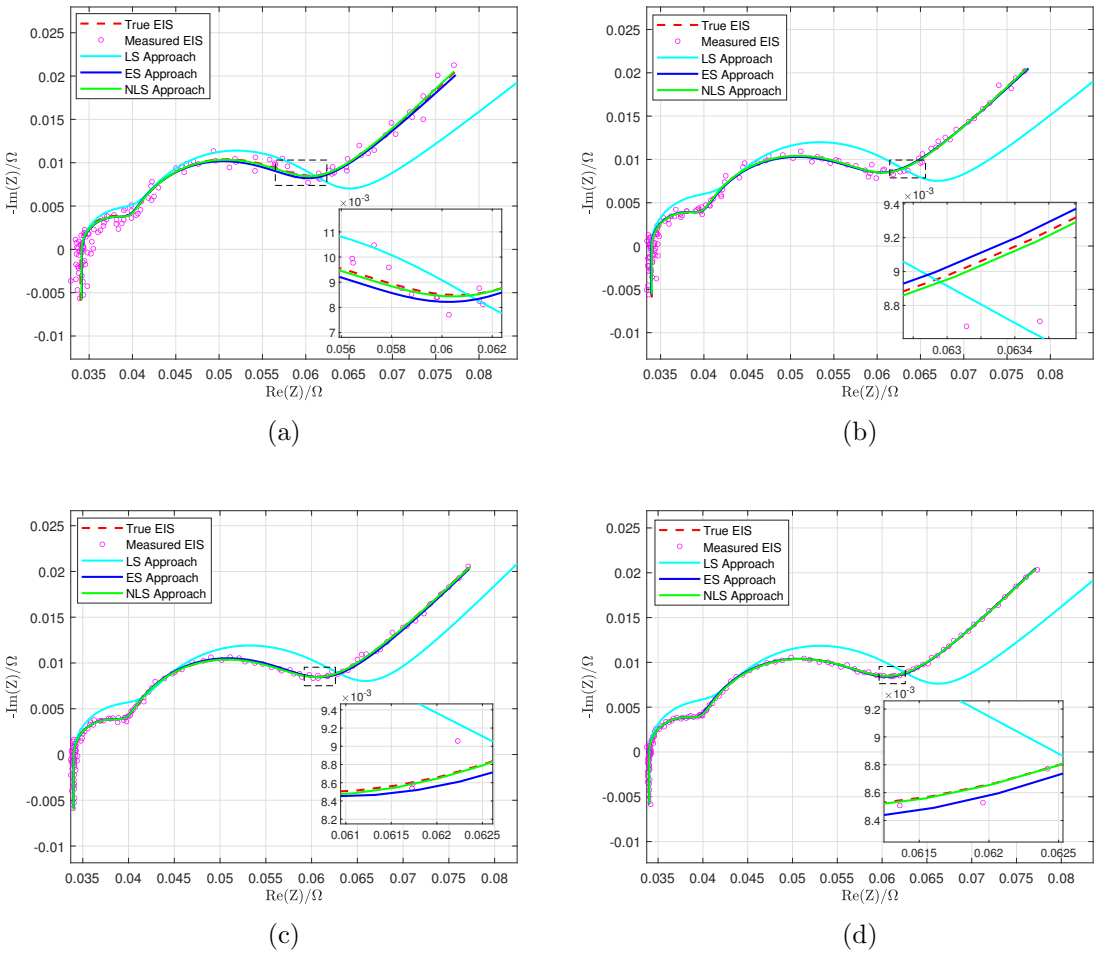


Figure 2.13: **Fitting simulated EIS measurements via LS, ES, and NLS approaches at different SNR.** (a) 35 dB. (b) 40 dB. (c) 45 dB. (d) 50 dB.

### 2.7.2 Estimation Results of ECM Parameters Using Real EIS Data

We selected LG 18650 and Molicel 21700 Li-ion batteries to validate whether the LS, ES, and NLS approaches show consistency in fitting real EIS data that are collected at 90%, 50%, and 10% SOC.

Fig. 2.15a, 2.15b, and 2.15c show the fitted EIS of LG 18650 battery using LS, ES, and NLS approaches; similarly, Fig. 2.15d, 2.15e, and 2.15f show the fitted EIS of Molicel battery using same approaches. It can be observed that the LS approach cannot fit the EIS data accurately in all cases; however, both ES and NLS approaches

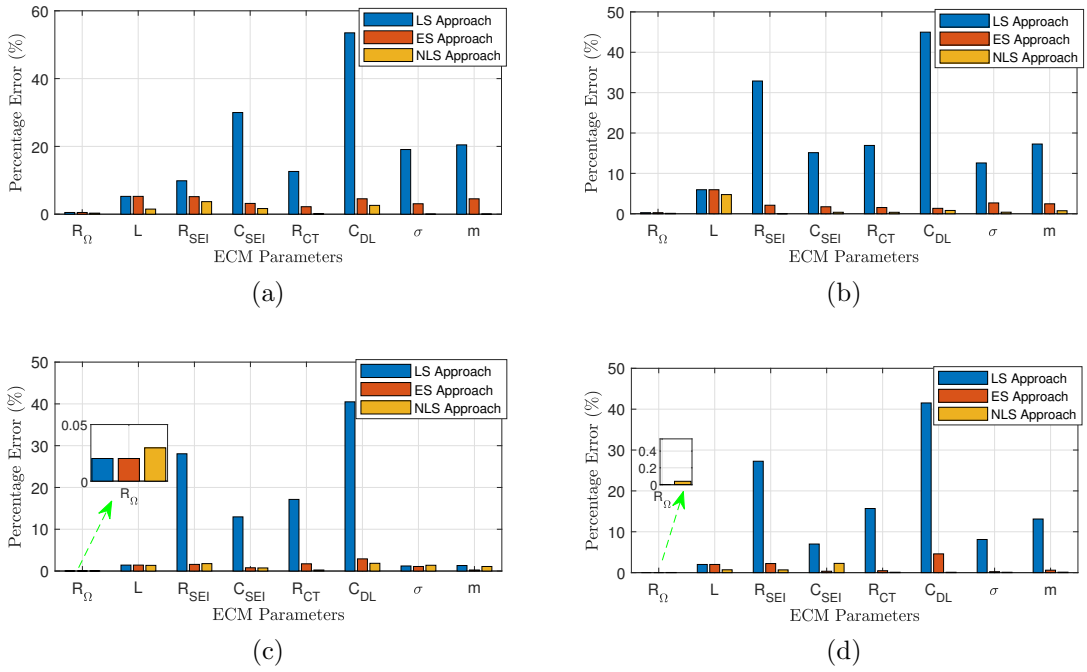


Figure 2.14: **Percentage difference between true and estimated ECM parameters at different SNR.** (a) 35 dB. (b) 40 dB. (c) 45 dB. (d) 50 dB.

show better goodness of fitting.

In Table 2.3, it can be observed that when fitting the LG battery's EIS data, the fitting accuracy of the ES approach is quite similar to that of the NLS approach, but at any SOC level, the EIS approach shows slightly better goodness of fitting; furthermore, comparing to the computational time, the ES approach considerably slower, whereas the NLS approach only needs around 2 seconds to fit the EIS data. Though the LS approach still shows the fastest computational time, the MAE is the highest among all SOC levels. Additionally, in Table 2.4, the validation on the Molicel battery shows consistent results.

## 2.8 Conclusion

This chapter presents the LS, ES, and NLS approaches to extract ECM parameters through battery impedance measurements. Compared to the LS approach, the ES

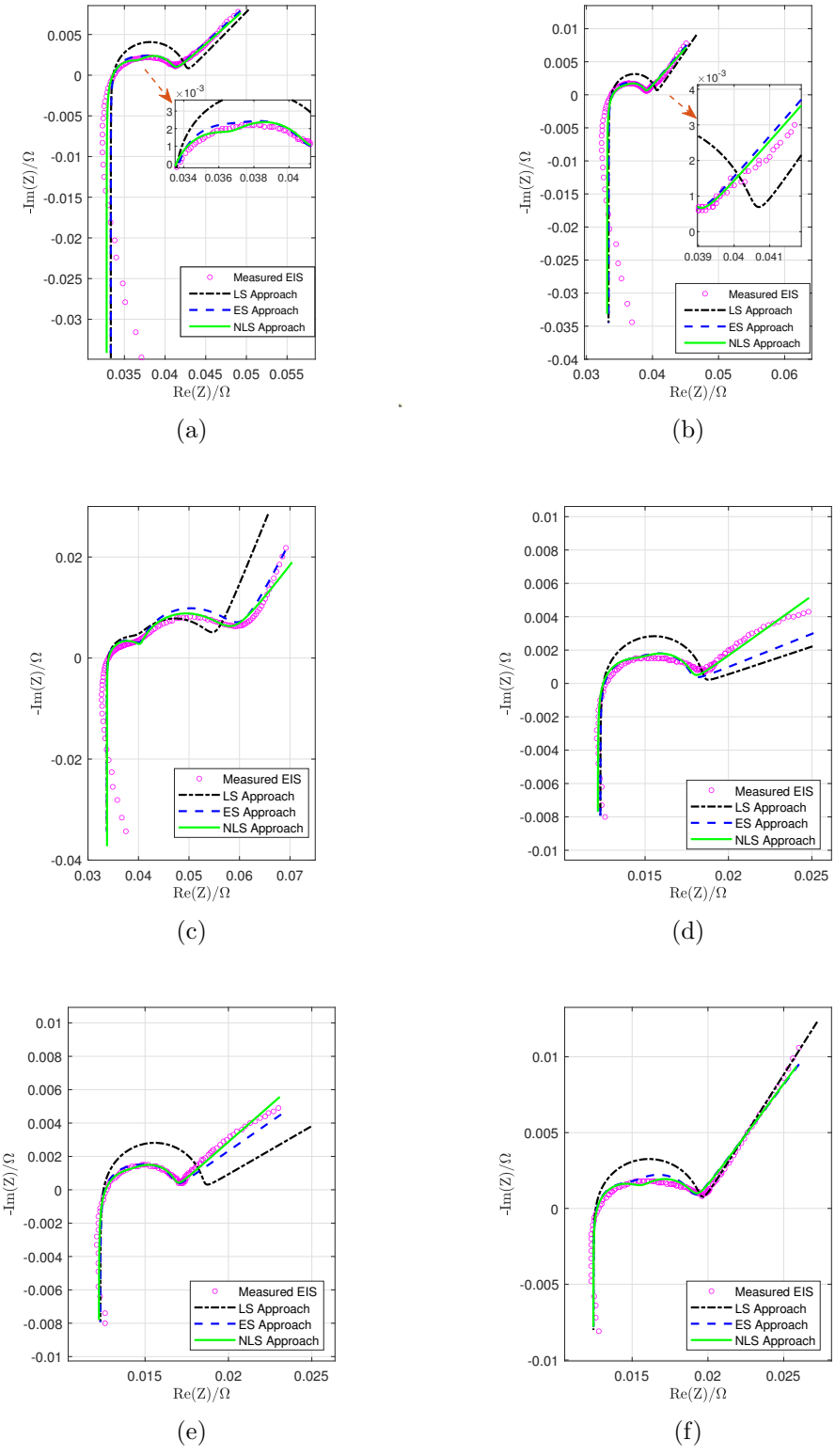


Figure 2.15: **Fitting real EIS measurements of LG and Molicel batteries at different SOC levels via LS, ES, and NLS approaches.** (a) LG battery at 90% SOC. (b) LG battery at 50% SOC. (c) LG battery at 10% SOC. (d) Molicel battery at 90% SOC. (e) Molicel battery at 50% SOC. (f) Molicel battery at 10% SOC.

Table 2.3: Estimated ECM parameters, computational time, and accuracy of using LS, ES and NLS approaches to fit real EIS data collected from LG 18650 battery while discharging

| **SOC** (%) | **Approach** | $\mathbf{R_\Omega}$ (mΩ) | **L** (nH) | $\mathbf{R_{SEI}}$ (mΩ) | $\mathbf{C_{SEI}}$ (F) | $\mathbf{R_{CT}}$ (mΩ) | $\mathbf{C_{DL}}$ (F) | $\boldsymbol{\sigma}$ ($\times 10^{-3}$) | **m** | **Runtime** (sec) | **MAE** ($\times 10^{-4}$) |
|---|---|---|---|---|---|---|---|---|---|---|---|
| 90 | LS | 33.3308 | 555.2298 | 4.8670 | 0.3253 | 4.1876 | 0.7179 | 1.9801 | 1.0186 | 0.729 | 16 |
| | ES | 33.3308 | 555.2298 | 3.7399 | 0.3253 | 3.6366 | 2.1536 | 2.1423 | 0.9221 | 133.9269 | 4.8733 |
| | NLS | 32.8162 | 544.9949 | 3.9102 | 0.1691 | 4.0532 | 1.9840 | 2.1418 | 0.8933 | 1.8634 | 3.9978 |
| 50 | LS | 33.3500 | 550.4295 | 3.9987 | 0.2971 | 3.0794 | 0.4795 | 1.5624 | 1.4540 | 0.7036 | 16 |
| | ES | 33.3500 | 550.4295 | 2.6938 | 0.2971 | 2.6742 | 1.2366 | 1.6223 | 1.1632 | 131.8468 | 4.1756 |
| | NLS | 33.1436 | 529.4929 | 2.8149 | 0.1890 | 2.8303 | 1.2932 | 1.5826 | 1.1364 | 1.7841 | 4.012 |
| 10 | LS | 33.7480 | 548.8295 | 6.3127 | 0.2972 | 14.3045 | 1.7628 | 2.8718 | 2.4868 | 0.7296 | 31 |
| | ES | 33.7480 | 548.8295 | 6.6449 | 0.2972 | 18.4450 | 5.1029 | 2.6614 | 1.9894 | 133.3339 | 12 |
| | NLS | 33.7766 | 593.9607 | 6.6475 | 0.2611 | 16.1871 | 5.2409 | 3.5550 | 1.3235 | 2.1813 | 9.3198 |

Table 2.4: Estimated ECM parameters, computational time, and accuracy of using LS, ES and NLS approaches to fit real EIS data collected from Molicel 21700 battery while discharging

| **SOC** (%) | **Approach** | $\mathbf{R_\Omega}$ (mΩ) | **L** (nH) | $\mathbf{R_{SEI}}$ (mΩ) | $\mathbf{C_{SEI}}$ (F) | $\mathbf{R_{CT}}$ (mΩ) | $\mathbf{C_{DL}}$ (F) | $\boldsymbol{\sigma}$ ($\times 10^{-3}$) | **m** | **Runtime** (sec) | **MAE** ($\times 10^{-4}$) |
|---|---|---|---|---|---|---|---|---|---|---|---|
| 90 | LS | 12.3167 | 128.0069 | 3.4751 | 0.1814 | 2.5873 | 0.3466 | 1.6716 | 0.3333 | 0.763 | 12 |
| | ES | 12.3167 | 128.0069 | 2.3411 | 0.1814 | 2.9278 | 1.0399 | 1.8852 | 0.4000 | 137.6328 | 5.8928 |
| | NLS | 12.1632 | 124.6571 | 2.5830 | 0.1318 | 2.9435 | 0.9523 | 1.7920 | 0.7169 | 1.8859 | 3.2337 |
| 50 | LS | 12.3167 | 128.0069 | 3.2931 | 0.1772 | 2.7962 | 0.3224 | 1.6401 | 0.5792 | 0.7237 | 15 |
| | ES | 12.3167 | 128.0069 | 2.2185 | 0.1772 | 2.1339 | 0.8994 | 1.6279 | 0.6950 | 135.3571 | 2.7111 |
| | NLS | 12.2259 | 126.3043 | 2.0331 | 0.1294 | 2.4749 | 0.7420 | 1.5924 | 0.8763 | 1.891 | 1.3862 |
| 10 | LS | 12.4444 | 129.6070 | 3.8936 | 0.1900 | 3.0673 | 0.3903 | 1.9573 | 1.5757 | 0.7366 | 12 |
| | ES | 12.4444 | 129.6070 | 2.6230 | 0.1900 | 3.7937 | 1.1708 | 1.7966 | 1.3269 | 134.0528 | 3.3286 |
| | NLS | 12.4349 | 126.2317 | 3.1777 | 0.1418 | 3.3352 | 1.9094 | 1.7361 | 1.3533 | 1.9071 | 2.7548 |

and NLS approach can extract ECM parameters more accurately. Furthermore, the presented novel NLS approach is based on the Monte Carlo run to fit the AR-ECM to the simulated and actual EIS measurements, which resulted in faster computation time and higher accuracy. When fitting the simulated EIS data, both ES and NLS approaches show considerably high accuracy when the SNR is low, and the fitting accuracy improves as the SNR increases. In contrast, the LS approach shows insufficient goodness of fitting at any SNR level. When fitting the actual EIS measurements collected from two different Li-ion batteries, the NLS approach still shows faster and more accurate fitting performance than the ES approach; this result is consistent with the validation in simulated EIS data. Though the ES approach shows acceptable accuracy, the computational time is considerably longer than the NLS approach.

Therefore, among the three proposed approaches, the best option is to apply the Monte-Carlo-based NLS approach to identify the ECM parameters through battery EIS.

## 2.9 Bibliography


[1] Z.-Y. Hou, P.-Y. Lou, and C.-C. Wang, "State of charge, state of health, and state of function monitoring for EV BMS," in *2017 IEEE International Conference on Consumer Electronics (ICCE)*, 2017.

[2] O. Heaviside, "Electrical papers by oliver heaviside (in two volumes)," *New York: MacMillon & Co*, vol. 268, 1894.

[3] P. Ranque, E. Gonzalo, M. Armand, and D. Shanmukaraj, "Performance-based materials evaluation for Li batteries through impedance spectroscopy: a critical review," *Mater. Today Energy*, vol. 34, no. 101283, p. 101283, 2023.

[4] S. R. Islam and S.-Y. Park, "Precise online electrochemical impedance spectroscopy strategies for li-ion batteries," *IEEE Transactions on Industry Applications*, vol. 56, no. 2, pp. 1661–1669, 2019.

[5] S. Mandal, P. Barai, P. Mukherjee, and R. Sharma, "An impedance-based study on the ageing of Li-ion batteries," *Electrochimica Acta*, vol. 307, pp. 161–174, 2019.

[6] H. Ju, J. Wu, and Y. Xu, "Revisiting the electrochemical impedance behaviour of the LiFePO4/C cathode," *J. Chem. Sci. (Bangalore)*, vol. 125, no. 3, pp. 687–693, 2013.

[7] C. Pastor-Fernández, W. D. Widanage, J. Marco, M.-Á. Gama-Valdez, and G. H. Chouchelamane, "Identification and quantification of ageing mechanisms in lithium-ion batteries using the eis technique," in *2016 IEEE Transportation Electrification Conference and Expo (ITEC)*, pp. 1–6, IEEE, 2016.

[8] N. Meddings et al., "Application of electrochemical impedance spectroscopy to commercial Li-ion cells: A review," *J. Power Sources*, vol. 480, no. 228742, p. 228742, 2020.

[9] M. Theiler, D. Schneider, and C. Endisch, "Experimental Investigation of State and Parameter Estimation within Reconfigurable Battery Systems," *J. Batteries*, vol. 9, no. 3, p. 145, Feb. 2023, doi: 10.3390/batteries9030145.

[10] N. Tian, Y. Wang, J. Chen, and H. Fang, "One-shot parameter identification of the Thevenin's model for batteries: Methods and validation," *J. Energy Storage*, vol. 29, no. 101282, p. 101282, 2020.

[11] J. Xu, L. Guo, Y. Liu, W. Li, Z. Li, and X. Zhang, "A non-linear least squares fitting method for analysis of electrochemical impedance spectroscopy data of a supercapacitor," *Journal of Energy Storage*, 2020.

[12] Y. Xu, X. Zheng, C. Wang, Z. Guo, C. Wang, and W. Wu, "Artificial Neural Network Based Electrochemical Impedance Spectroscopy Modeling for Lithium-Ion Batteries," *Journal of Electrochemical Energy Conversion and Storage*, vol. 16, no. 4, 2019.

[13] X. Li, C. Chen, X. Lü, W. Zhang, J. Liu, and H. Yu, "A review on the applications of electrochemical impedance spectroscopy in batteries," *Journal of Energy Chemistry*, vol. 53, pp. 146–162, 2021.

[14] F. Feng et al., "Electrochemical impedance characteristics at various conditions for commercial solid–liquid electrolyte lithium-ion batteries: Part. 2. Modeling and prediction," *Energy (Oxf.)*, vol. 243, no. 123091, p. 123091, 2022.

[15] Y. Liu, Y. Cai, T. Gao, and H. Liu, "Comparison of different methods for fitting equivalent circuit models to EIS data of lithium-ion batteries," *Electrochimica Acta*, vol. 343, 2020.

[16] M. A. Ghadi, *Performance Analysis and Improvement of Electrochemical Impedance Spectroscopy for Online Estimation of Battery Parameters*, Master's thesis, University of Windsor, Windsor, ON, Canada, 2021.

[17] S. Wang, J. Zhang, O. Gharbi, V. Vivier, M. Gao, and M. E. Orazem, "Electrochemical impedance spectroscopy," *Nat. Rev. Methods Primers*, vol. 1, no. 1, pp. 1–21, 2021.

[18] E. Barsoukov and J. R. Macdonald, Eds., "Impedance Spectroscopy; Theory, Experiment, and Applications," *Wiley Interscience Publications*, 2005.

[19] M. E. Orazem and B. Tribollet, "Electrochemical impedance spectroscopy," *New Jersey*, pp. 383–389, 2008.

[20] B. Balasingam and K. R. Pattipati, "On the identification of electrical equivalent circuit models based on noisy measurements," *IEEE Transactions on Instrumentation and Measurement*, vol. 70, pp. 1–16, 2021.

[21] W. Waag, S. Käbitz, and D. U. Sauer, "Experimental investigation of the lithium-ion battery impedance characteristic at various conditions and aging states and its influence on the application," *Applied energy*, vol. 102, pp. 885–897, 2013.

[22] Y. Wu, S. Sundaresan, and B. Balasingam, "Battery parameter analysis through electrochemical impedance spectroscopy at different state of charge levels," *J. Low Power Electron. Appl.*, vol. 13, no. 2, p. 29, 2023.

[23] M. Baum, V. Klumpp, and U. D. Hanebeck, "A novel Bayesian method for fitting a circle to noisy points," in *2010 13th International Conference on Information Fusion*, 2010.

[24] T. F. Coleman and Y. Li, "An Interior, Trust Region Approach for Nonlinear Minimization Subject to Bounds," *SIAM Journal on Optimization*, vol. 6, pp. 418–445, 1996.

[25] T. F. Coleman and Y. Li, "On the Convergence of Reflective Newton Methods for Large-Scale Nonlinear Minimization Subject to Bounds," *Mathematical Programming*, vol. 67, no. 2, pp. 189–224, 1994.

[26] K. Levenberg, "A Method for the Solution of Certain Problems in Least-Squares," *Quarterly Applied Mathematics*, vol. 2, pp. 164–168, 1944.

[27] D. W. Marquardt, "An algorithm for least-squares estimation of nonlinear parameters," *J. Soc. Ind. Appl. Math.*, vol. 11, no. 2, pp. 431–441, 1963.

[28] J. J. Moré, "The Levenberg-Marquardt Algorithm: Implementation and Theory," *Numerical Analysis*, vol. 630, pp. 105–116, 1977.

[29] F. Vanden Berghen, "Levenberg-Marquardt algorithms vs Trust Region algorithms," *Applied-mathematics.net*, [Online]. Available: http://www.applied-mathematics.net/LMvsTR/LMvsTR.pdf. [Accessed: 04-Aug-2023].

[30] *Instrument Operator's Manual*, Gamry Instruments Inc, EIS Box, 2018.

[31] "LPI1010 High Voltage Test System for EIS up to 20kHz Gamry instruments," *Gamry.com*, [Online]. Available: https://www.gamry.com/news-and-announcements/general-news/high-voltage-test-system/. [Accessed: 10-Jul-2023].

[32] M. Welvaert and Y. Rosseel, "On the definition of signal-to-noise ratio and contrast-to-noise ratio for FMRI data," *PLoS One*, vol. 8, no. 11, p. e77089, 2013.

# Chapter 3

# Thesis Conclusion

This thesis introduced the process of measuring battery impedance response and its graphical representation; and, most importantly, using the presented LS, ES, and NLS approaches to extract ECM parameters through battery impedance measurements from simulation data and actual EIS data collected from LG 18650 and Molicel 21700 batteries. Compared to the LS approach, the ES and NLS approaches reveal superior accuracy in ECM parameter extraction. Notably, the novel NLS approach incorporates Monte Carlo simulations to fit the AR-ECM to simulated and actual EIS measurements, resulting in faster computation time and higher accuracy. For simulated EIS data, the ES and NLS approaches demonstrate remarkable accuracy even under low signal-to-noise ratio (SNR) conditions, with improved fitting precision as the SNR increases. Conversely, the LS approach fails to provide satisfactory fitting quality across all SNR levels. When applied to actual EIS measurements collected from the two different Li-ion batteries, the NLS approach consistently outperforms the ES approach regarding both fitting speed and accuracy, corroborating the findings from the validation via simulated EIS data. While the ES approach exhibits acceptable accuracy, its computational time is significantly longer compared to the NLS approach. Therefore, considering the results obtained from the three proposed approaches, the Monte-Carlo-based NLS approach emerges as the optimal choice for

identifying ECM parameters through battery EIS.

## Future work

In future works, we will investigate deploying the NLS approach to the BMS board combined with the rapid EIS measurement hardware to improve the accuracy and computational time for ECM parameters estimation; the BMS can then adopt these precisely estimated ECM parameters for more accurate online SOC/SOH estimation.

# Vita Auctoris

| | |
|---|---|
| NAME: | Yuchao Wu |
| PLACE OF BIRTH: | Shiyan, China |
| YEAR OF BIRTH: | 1991 |
| EDUCATION: | University of Windsor<br>Windsor ON, Canada<br>2020-2021, Master of Engineering<br>Mechanical Engineering<br><br>University of Windsor,<br>Windsor ON, Canada<br>2022-2023, Master of Applied Science<br>Electrical Engineering |